NASA
TM
X-63533
c.1

TECH LIBRARY KAFB, NM
0152386

N69-25156

A SYSTEM TO MONITOR STELLAR IMAGE QUALITY

Jack L. Bufton

Goddard Space Flight Center
Greenbelt, Maryland

March 1969

DISTRIBUTED BY: CLEARINGHOUSE
FOR FEDERAL SCIENTIFIC AND TECHNICAL INFORMATION

U. S. DEPARTMENT OF COMMERCE / NATIONAL BUREAU OF STANDARDS / INSTITUTE FOR APPLIED TECHNOLOGY

YOUR KEY...

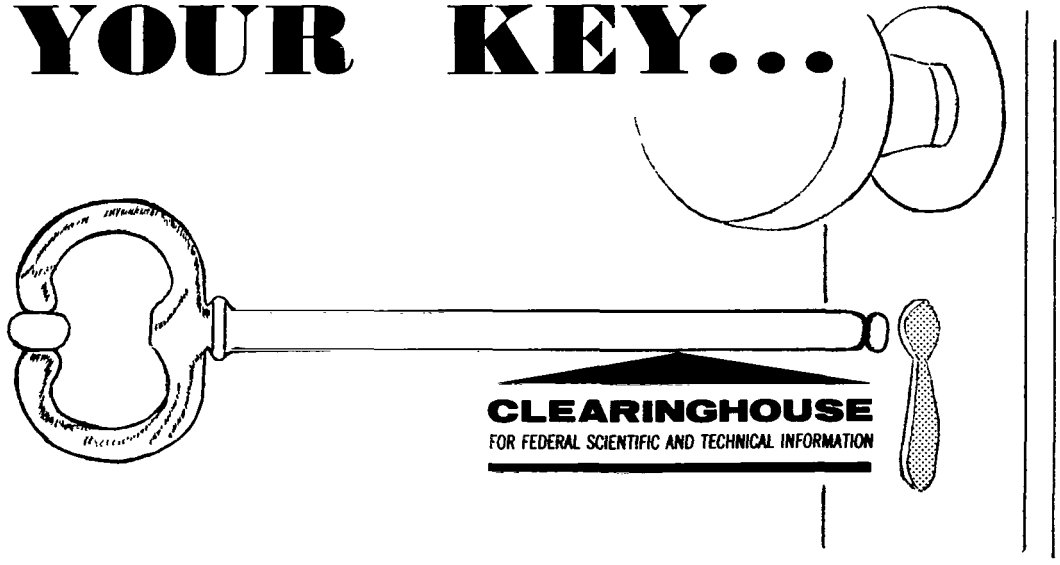

to scientific and technical advancement

Mr. Scientist. . .Engineer. . .Businessman. . .the Clearinghouse for Scientific and Technical Information can serve as your key to progress in research and development. Each year, some 40,000 unclassified documents from more than 125 Government agencies enter our collection. The Clearinghouse announces, reproduces and sells these reports to the public at a nominal cost. To make this wealth of scientific and technical information readily available, we have tailored our services to meet the needs of the highly selective customer as well as the general user. Some of these services are listed below.

U.S. GOVERNMENT RESEARCH AND DEVELOPMENT REPORTS (USGRDR). This semimonthly journal abstracts approximately 40,000 new Government-sponsored reports and translations annually. Features a quick-scan format, cross references, edge index to subject fields, and a report locator list.

U.S. GOVERNMENT RESEARCH AND DEVELOPMENT REPORTS INDEX (USGRDR-I). Published concurrently with the USGRDR to index each issue by subject, personal author, corporate source, contract number and accession/report number. Quarterly Indexes and an Annual Cumulative also are available.

CLEARINGHOUSE ANNOUNCEMENTS IN SCIENCE AND TECHNOLOGY. A semimonthly current awareness announcement service in 46 separate categories representing complete coverage of all documents announced by the Clearinghouse. Highlights special interest reports.

FAST ANNOUNCEMENT SERVICE (FAS). Selective announcement service emphasizing commercial applications of report information. Covers approximately 10 percent of Clearinghouse document input. Compiled and mailed in 57 categories.

SELECTIVE DISSEMINATION OF MICROFICHE (SDM). Automatic distribution twice monthly of Government research and development reports on microfiche. Economical and highly selective. Several hundred categories from which to choose.

ADDITIONAL INFORMATION concerning these and other Clearinghouse services is available by writing to:

Customer Services
Clearinghouse
U.S. Department of Commerce
Springfield, Virginia 22151

X-524-69-101

PREPRINT

NASA TM X- 63533

A SYSTEM TO MONITOR STELLAR IMAGE QUALITY

N69-25156

(ACCESSION NUMBER) 118 (PAGES) | (THRU) 1 | TMX 63533 (NASA CR OR TMX OR AD NUMBER) | (CODE) (CATEGORY) 14

FACILITY FORM 602

JACK L. BUFTON

MARCH 1969

GODDARD SPACE FLIGHT CENTER

GREENBELT, MARYLAND

X-524-69-101

PREPRINT

A SYSTEM TO MONITOR STELLAR

IMAGE QUALITY

Jack L. Bufton

March 1969

GODDARD SPACE FLIGHT CENTER

Greenbelt, Maryland

TECH LIBRARY KAFB, NM

0152386

PRECEDING PAGE BLANK NOT FILMED.

A SYSTEM TO MONITOR STELLAR IMAGE QUALITY

Jack L. Bufton

Optical Systems Branch

Advanced Development Division

ABSTRACT

The following report outlines the development and implementation of a systematic approach to measurement of stellar image quality in a turbulent atmosphere. The concept is that of J. V. Ramsay and H. Koebler, C.S.I.R.O., Sydney, Australia. Simultaneous but independent measures are made of total intensity, size, and movement of the stellar image. The critical parameter of image size is deduced from a Fourier transformation of optical spread function in the focal plane of a six inch diameter telescope. This results in an optical transfer function for the atmosphere and telescope optics. Experimental hardware has been developed and field tested at Goddard Optical Research Facility. Data is recorded in the field on magnetic tape and later processed by digital computer. In this project most emphasis is placed on data reduction and interpretation with the aim of developing a capability to evaluate particular sites for their image quality and to make meaningful comparisons with current theories on optical propagation.

ECEDING PAGE BLANK NOT FILMED.

CONTENTS

APPENDICES

ILLUSTRATIONS

ACKNOWLEDGMENTS

The author wishes to express his appreciation to Michael W. Fitzmaurice and Peter O. Minott, Optical Systems Branch, Goddard Space Flight Center and Dr. Douglas G. Currie, University of Maryland for their guidance during the development of this experiment and to John W. Larmer and David A. Grolemund, Bendix Field Engineering Corporation for their technical assistance.

A SYSTEM TO MONITOR STELLAR IMAGE QUALITY

SECTION I

INTRODUCTION

A device to monitor the quality of stellar images has been selected and developed by the Optical Systems Branch. The device and its experimental program have been designed to meet the following objectives:

(1) Development of techniques to monitor atmospheric effects on vertical propagation of optical radiation

(2) Recording of data on the optical quality of the atmosphere at particular sites, such as the Goddard Optical Research Facility and Mt. Hopkins, Arizona

(3) Relation of data to theoretical analysis of atmospheric effects at optical frequencies.

The OTTOS Study Report of June, 1967, emphasized NASA's long standing need for a field facility to house and operate the Agency's growing capability in optical tracking and communication. As a necessary beginning, the report recommended an active program of atmospheric research and testing for site selection and evaluation. More recently, attention has been focussed on NASA use of the SAO Southwest Observatory at Mt. Hopkins, Arizona, on a cooperative basis. Thus, plans for the Goddard Stellar Image Monitor (SIM) and other site

testing instruments were directed toward the specific goal of evaluating the Mt. Hopkins site. Primary emphasis was placed on quantitative data and meaningful comparisons with theory.

The process of site evaluation for optical communication purposes closely parallels the site evaluation task in astronomy. Both cases require the input of information from many areas, the specification of atmospheric propagation characteristics being only one of the most important. Optical characteristics of a site include many parameters, such as cloud cover, aerosol content, infrared transparency, resolution of stars, and sky background. A lack of perfection in these measurable parameters can be attributed to three mechanisms at work in the atmosphere: absorbtion, molecular and aerosol scattering, and turbulence-induced scattering. The first two mechanisms result in effects that can be minimized or eliminated by proper choice of site. In addition, they are relatively steady-state effects, not varying significantly within a particular locality or length of time. The third mechanism, turbulence, results in the most serious optical problems. The unstable, and as yet quite unpredictable turbulent processes, produce random fluctuations in refractive index along the optical path. This in turn distorts the phase or shape of the optical wavefront and causes variations in irradiance across the wavefront. These distortions vary strongly over short periods of time and among different locations at a particular site.

For vertical atmospheric paths, measurements of starlight yield information on optical wavefront distortions. Starlight is collected by telescope optical systems, and the quality of the image examined. This closely parallels the detection

of light from spaceborne laser systems by observers on the earth, an essential ingredient of optical communication. Astronomers have long been aware of degradation of stellar image quality and classed the effects as scintillation, dancing, pulsation, shimmer, boil and focus shift. Together these effects constitute "seeing" through the atmosphere. More compactly, they may be grouped into image intensity variations and fluctuations in the size, position, and symmetry of the image. Until recently, measures of "seeing" have been semi-quantitative at best. Often, a scale of one to five has been used to distinguish periods of good and bad "seeing". The evaluation of a site for optical communication requires a more exact measure of image quality.

In the Stellar Image Monitor Experiment, image quality is determined from data on image intensity, size, and position. Data on image intensity fluctuations or scintillation is taken simply by photoelectric detection of total light in the image. However, size and position fluctuations of stellar images, which bear most directly on their quality, are not so easily measured. Fortunately, the data taking and analysis procedures are simplified by use of optical transfer functions. This is the method employed by the SIM Experiment.

Use of transfer functions is a powerful technique especially suitable for optical communication. A transfer function in communication theory reveals a system's ability to transmit information. That is, it predicts the response for a given input. In optical communications, the information will be a form of encoding on the optical beam. The atmospheric medium will distort the encoding

as will the transmission and detection process. If all processes are described by transfer functions, they can be simply combined to describe total system performance. The optical transfer function has the additional advantage of predicting specific parameters such as photographic resolution and optical heterodyne signal-to-noise ratio.

The transfer function of an optical system is defined as the two-dimensional spatial Fourier transform of the image spread function. The magnitude of the transfer function is a measure of the reduction in contrast suffered by each Fourier component of the object after transmission through the entire imaging system. It is a function of the transform variable, spatial frequency, which is expressed in cycles per unit length or cycles per radian field of view in the focal plane.

$$T(\vec{f}) = \int_{-\infty}^{\infty} \int_{-\infty}^{\infty} s(\vec{x} - \vec{x}'; \lambda) \exp(-2\pi i \vec{f} \cdot \vec{x}) \, d\vec{x} \qquad (1)$$

$T(\vec{f})$ = optical transfer function

$S(\vec{x} - \vec{x}'; \lambda)$ = image spread function

For the particular case represented by starlight (point source and incoherent light), the optical transfer function (OTF) is just the Fourier transform of the

image intensity distribution.[1]

$$T(\vec{f}) = \int_{-\infty}^{\infty} \int_{-\infty}^{\infty} I(\vec{x}) \exp(-2\pi i \vec{f} \cdot \vec{x}) \, d\vec{x} \qquad (2)$$

$\vec{x}$ = two dimensional vector in focal plane

$I(\vec{x})$ = image profile

$\vec{f}$ = two dimensional spatial frequency vector

The magnitude or modulus of $T(\vec{f})$ is the quantity measured in the SIM. In electronic terms, useful for handling data, modulus is equal to modulation index, a number between zero and one. The Fourier transform inversion formula expresses image intensity profile in terms of $T(\vec{f})$.

$$I(\vec{x}) = \int_{-\infty}^{\infty} \int_{-\infty}^{\infty} T(\vec{f}) \exp(2\pi i \vec{f} \cdot \vec{x}) \, d\vec{f} \qquad (3)$$

$T(\vec{f})$ = optical transfer function

Both phase and amplitude effects in the atmospherically distorted wavefront contribute to $T(\vec{f})$. Phase changes can be thought of as tilts or bends in the wavefront and lead to a blurred image. Additional diffraction and consequent image blurring is due to wavefront amplitude effects. These effects can be considered a random apodization of the telescope lens. The blurring transfer function is measured in the Stellar Image Monitor (SIM) for the optical system

[1] Appendix A contains the assumptions and mathematical analysis relating OTF and image intensity profile.

composed of the atmosphere and telescope optics. Laboratory test data enables the telescope optics transfer function to be separately determined. This function results from diffraction at the lens aperture and from the effect of any aberrations present.

Besides blurring, images are also observed to fluctuate in position or dance. The SIM measures motion of image center of gravity as the third ingredient of image quality. Movements are caused by wavefront phase changes, primarily tilts. A transfer function for image motion may be constructed from the data and combined with the blurring function to yield a combined transfer function for the atmospheric part of the optical system. Section IV of this document will be concerned with relation of the transfer functions and the three data outputs of the SIM to atmospheric theory and engineering parameters.

SECTION II

STELLAR IMAGE MONITOR DESIGN AND OPERATION

CONCEPT

The Goddard SIM is based on a design published by Ramsay (Reference 18) and a technique described by Lindberg (Reference 15). Ramsay performed some experimental work with starlight and later Coulman (References 2 and 3) used the device extensively for horizontal optical propagation studies. The SIM generates an OTF by performing a Fourier transform on the image intensity distribution in the focal plane of a telescope. The transform is generated by square

wave chopping the image at a selected but variable spatial frequency. Operation at different spatial frequencies allows the entire OTF of the atmosphere plus telescope optics to be measured. The Goddard device differs in the way spatial frequency is varied, in the pre-processing electronics, and in data collection and reduction. At Goddard, most emphasis is placed on data reduction and interpretation. Data recorded in the field on magnetic tape is later analyzed by digital computer. The computer is programmed to output a virtually written statistical record of the recorded data. A detailed account of this important process is given in Section III. Figure 1 illustrates the experiment concept and Figure 2 is a photograph of the equipment used.

OPTICAL SYSTEM AND DETECTOR PACKAGE

In the SIM, starlight is collected by a six inch diameter doublet lens system of 48 inches focal length. Figure 3 indicates the optical system components. As converging starlight enters the experiment package, it encounters a partially silvered mirror. This surface, acting as a beamsplitter, allows 30% of the light to pass through and reflects 60%. Transmitted light enters a penta-prism and is directed through a corrector plate to focus on a ring and cross-line reticle. The field of view corresponding to the ring's diameter is 14 minutes of arc. Observation of the stellar image on the reticle allows pointing of the telescope to insure on axis operation. Light reflected by the beamsplitter is reflected again by a front surface mirror and allowed to come to focus. A microscope objective serves as relay optics to focus an enlarged image of star on a rotating

glass disk. An eyepiece and mirror assembly mounted in a sliding tube are used to visually check image quality and insure proper alignment of the image on the glass disk. The disk is composed of alternate clear and opaque pie-shaped sectors as detailed in Figure 3. Each sector subtends one-half degree. The pattern was produced at Goddard by photographic-reduction and etching from a machine drawn original. The disk is belt driven from a D.C. motor-servo system at a constant rate of 517 rpm. Speed regulation is better than .5%. Light passing through the disk is thus square-wave modulated with a time frequency of 3.1 KHz, determined by motor speed and number of sectors on the disk. The spatial frequency of chopping is inversely proportional to the distance from the center of the disk and is determined by sector width at a given distance. Since a clear and opaque sector determine one cycle of chopping, the spatial frequency in cycles per millimeter is the reciprocal of the width of two sectors. Spatial frequency can be made independent of lens parameters by multiplication by system focal length. Cycles per mm become cycles per radian field of view or cycles per arc second. Starlight is brought to a focus one inch from the center of the disk. For unity power relay optics the spatial frequency of chopping is 2.26 cycles per mm or .0134 cycles per arc second. Higher powers effectively increase the spatial frequency by enlarging the image on the disk. Below are listed the linear increases in spatial frequency achieved with various powers of microscope objective.

Table 1

Microscope Objective Power and Spatial Frequency

Microscope Objective Power	Spatial Frequency (Cycles/Arc Second)
1	.0134
2.6	.0348
3.5	.0469
4.0	.0536
6.0	.0803
10	.134
21	.281
45	.602
60	.803
98	1.31

Light transmitted by the disk passes through an optical highpass filter and is received by a photomultiplier tube. The photomultipiler tube is an RCA Model 6199 with S-11 response. The filter is a Corning glass filter number CS-72. The combined spectral response is approximately 1200Å centered at 5000Å (Figure 4).

Light from a small D.C. powered lightbulb is also focussed on the disk to act as a phase reference source. A thin glass plate in the converging light from the bulb can be tilted to adjust the position of this image on the disk. Chopped

light is received by a PIN 10 photodiode. A field effect transistor preamplifier and biasing network prepares the photodiode signal for entry into the electronic preprocessing system. The photomultiplier signal is developed across a one megohm load resistance and unity gain preamplifier stage.

PROCESSING ELECTRONICS

Electrical signals from the two detectors are fed into an electronic preprocessing system[1] (Figure 5). The main function of this device is to produce three voltages containing information on image intensity, modulation index, and motion. Burr Brown integrated circuit operational amplifiers, Model 3052, are the primary circuit constituent. The entire instrument is D.C. powered by either a regulated power supply or battery providing 24 to 28 volts at approximately .2 amps. Solid state voltage regulators provide the plus and minus 12 volts required for operational amplifier biasing. In addition, a programmable D.C. to D.C. converter provides up to 2000 volts for the photomultiplier tube. The converter is a Venus Scientific K150B rated at 1 milliamp D.C.

The positive going input from the photomultiplier preamplifier stage is in the form of an amplitude and frequency modulated square wave at the chopping frequency, 3.1 KHz. This signal and the photodiode signal are not perfect square waves since image size is not negligible compared to sector width. Only the fundamental sine wave component of the square wave is of interest, however. As shown in Figure 5, the photomultiplier signal proceeds through two inverting

[1]Developed under contract to NASA–GSFC by Fairchild Hiller Corporation, Bladensburg, Maryland.

D.C. amplifier stages. The first has a gain of ten and the second incorporates a variable gain from one of twenty. At this point, the amplified signal proceeds two ways. The first path is through a low pass filter of the multiple feedback design having a corner frequency of 200 Hz. The filter's output is just the measurement of total image intensity and its scintillation. This D.C. or low frequency information output 1, is also used in the determination of modulation index. The second path is through a multiple feedback bandpass filter centered at the chopping frequency. This frequency belongs to the fundamental sinusoidal component in the square wave. The 3 db bandwidth of the filter is plus or minus 200 Hz. around the center frequency. A Transmagnetics Model 480CP5 analog divider receives the outputs of both filters and performs the operation A.C. divided by D.C. The output of the divider is the normalized chopping frequency component; that is, the strength of the component with respect to D.C. As the image size grows larger due to turbulence or as spatial frequency is increased, the A.C. component suffers a reduction. Size changes affect only the A.C. component while intensity changes or scintillation are present in both A.C. and D.C. components and cancel out in the division process. The divider's output is received by a peak detector which produces a D.C. voltage, output 2, proportional to the modulation index or relative strength of A.C. to D.C. Fluctuations in modulation index can be followed from D.C. to the corner frequency of 200 Hz. If the peak value of A.C. is equal to the D.C. signal strength, the modulation index is 1.0.

Motion of image center of gravity is determined by phase comparison of signals at the chopping frequency, 3.1 KHz, from the two detectors. As the stellar image moves on the chopping disk, it produces a waveform shifted in phase with respect to that from the phase reference source with its stationary image. The preamplified reference signal from the photodiode is first sent through a bandpass filter identical to that used in processing the phototube signal. The outputs of both bandpass filters are sent through limiter stages to provide good clean square waves. A Fairchild UA702A integrated circuit phase comparator receives the square waves and outputs a pulse train whose duty cycle is proportional to the relative phase of the signals. An RC averaging network with response from D.C. to the corner frequency of 200 Hz. measures the duty cycle. Relative phase of the two signals is just the relative position of the two images on the disk along a direction perpendicular to a disk radius. Thus, output 3 becomes a voltage proportional to one-dimensional motion of stellar image center of gravity.

The results of electronic and optical calibration tests of the preprocessing system are given in Section V. These tests were necessary to insure proper operation of the electronics and to relate the voltage outputs to parameters specifying image quality.

DATA COLLECTION

In order to preserve the output data of the electronic preprocessing system in a form suitable for data analysis, recordings are made on magnetic tape. For this purpose, an Ampex FR-1300 portable instrumentation tape recorder has

been incorporated into the system. This is a seven track machine equipped in a standard IRIG configuration for one-half inch wide magnetic tape. The three outputs of the electronic pre-processing system have bandwidths from D.C. to 200 Hz. The D.C. requirement means a frequency modulation (FM) recording scheme must be used. Time signals are also recorded in order to properly characterize and identify the data. The NASA one per second and one per minute binary time codes are the ones used. These can be recorded in the direct (AM) mode. Recording is done at a tape speed of 7.5 inches per second. The FM and AM record bandwidths are from D.C. to 2.5 KHz and from 50 Hz. to 38 KHz, respectively. A 10 KHz sine wave is also recorded in the direct mode as a reference signal. Tape speed errors made in data taking can be eliminated during automatic data processing by using the 10 KHz reference signal. Such errors would result from fluctuations in power line frequency, a common occurrence in remote locations where power is obtained from portable generators. A complete set of tape recorder specifications is included in Appendix C.

Operation of the Stellar Image Monitor Experiment involves nighttime stellar observations at various zenith angles, azimuths, and for various times of night. Two operating personnel are required: one to adjust telescope pointing and optical alignment, the other to monitor the electronics and operate the tape recorder. In acquiring a star, successive use is made of a wide field viewfinder and narrow field, high power eyepiece. This insures operation of the telescope on-axis. The focussing and centering microscope objective holder is then used

to bring the stellar image to the correct focus and position on the chopper wheel. This process is monitored by the sliding eyepiece. After proper alignment is achieved, the eyepiece is removed and starlight enters the detector package. Once the photomultiplier high voltage control and D.C. amplifier gain have been adjusted for the proper intensity output voltage, the instrument is ready for data recording.

Data taking procedures are tailored closely to the demands of data reduction. To this end, calibration voltages, a star identification code, and background runs are recorded on magnetic tape along with the data, time, and reference signals (see Figure 5). A voice edge track is used to note experimental parameters such as spatial frequency, telescope aperture, photomultiplier tube high voltage, and amplifier gain. Data taking is divided for convenience into four distinct categories. A tape is the largest category. It is the contents of one reel (2,500 feet) of magnetic tape and may include data from several nights, the second category. The third level is called a star. It includes all data taken in succession with a particular stellar source. Included here may be from one to ten data runs, the final category.

A data run begins when the tape recorder is turned on and ends with tape recorder off. It is characterized by a three digit data run number and a particular spatial frequency. Nominal operation would include six data runs per star; each conducted at a different spatial frequency. Below is listed the format of a data run. An example is given in Figure 6.

Table 2

Data Run Format

Event Number	Event	Length (Seconds)
	START RECORDER	
1.	Tape leader at ground potential	20
2.	Positive six volts calibration	10
3.	Ground potential	5
4.	Negative six volts calibration	5
5.	Star number hundreds digit	3
6.	Star number tens digit	3
7.	Star number units digit	3
8.	Data	10 to 600
9.	Defocus data	5
10.	Background data	5
	STOP RECORDER	

The first seven events are fed automatically to the tape recorder by a commutator arrangement. The commutator selects the desired D.C. voltage level for the specified length of time. Tape leader allows time for the tape recorder transport mechanism to come up to speed and stabilize. Known calibration voltages are recorded to provide a voltage standard in data reduction. The three star numbers are the hundreds, tens, and units digits that comprise the number assigned to a particular star. This number may be found in Apparent Places of

Fundamental Stars. Each digit is a certain percentage of plus calibration voltage. For example, the star number 297 would comprise voltage levels 20%, 90%, and 70% respectively of plus calibration. Actual star data is taken from ten seconds to ten minutes. Defocus data is generated when the telescope operator deliberately defocuses the stellar image on the chopper wheel. This is used to characterize the modulation index data. Background data requires the operator to point the telescope so that the star is just beyond the field of view. Thus, all the effects of stray light, sky background, and electronic offset can be recorded.

Data from the three outputs of the SIM is recorded simultaneously in each data run. Time and reference signals are recorded continuously without the calibration voltages and star code. Below is a listing of the seven tracks of the magnetic tape recorder, their function, and mode of recording.

Table 3

Tape Recorder Format

Track Number	Function	Record Mode
1	Spare	FM
2	10 Kllz reference	AM
3	Image motion data	FM
4	Intensity data	FM
5	Modulation index data	FM
6	BCD time code 36 bit	AM
7	BCD time code 28 bit	AM

The electronic equipment described above is mounted in a standard five foot instrumentation rack as shown in detail in figures 7 and 8. The following items are included.

1. Electronic preprocessing system
2. Calibration voltage commutator
3. Tektronix type 422 oscilloscope
4. Newport Labs series 200 digital panel meter
5. Trygon HR40-3B D.C. power supply
6. Electro-Craft E-650 motor speed control system
7. Ampex FR-1300 instrumentation tape recorder

The oscilloscope and digital panel meter are used to monitor signal levels during data recording. Time and reference signals must be fed into the rack from an external time code generator. Appendix C contains selected manufactures data on the critical electronic components.

SECTION III

DATA REDUCTION

The Goddard concept of the Stellar Image Monitor Experiment places most emphasis on data reduction and interpretation. What previously involved many tedious hours of manual data reduction from chart recordings has been perfected to an automated process using high speed digital computers. Data recorded on magnetic tape in the field is transported to the GSFC computing facility where

automatic routines digitize the information and read it into a computer. There the main program takes over, operates on the data, and outputs virtually written statistical records. Output is presented in tabular and graphical form for ease of data interpretation.

The three outputs of SIM are randomly fluctuating voltage levels representing optical fluctuations in the stellar image being monitored. Similar to the atmospheric mechanisms reponsible, these optical fluctuations have a large dynamic range and periods as short as several milliseconds. In Figure 9 sample chart recordings of each of the three data tracks are presented. Clearly, one must turn to statistics in order to characterize the data. Consideration must be given to averages, variances, correlations, and power spectrums.

COMPUTER STATISTICAL ANALYSIS

Once data has been recorded on magnetic tape, the first step in data reduction converts the information into a digital format. For this, the facilities of the Information Processing Division at GSFC are used. Analog data tapes are played back through an analog to digital (A/D) conversion unit and digital tapes are produced. A/D sampling is at a rate of 4KHz. A sample is taken every quarter millisecond. The data tracks are sampled sequentially with the net result that each of the three outputs of the SIM plus a spare fourth track are sampled every millisecond. Fundamental sampling theorems require that the sampling rate be twice the highest frequency component in the data. This insures correct representation in digital form of the original data. Sampling 1000 times per second

allows the data to contain frequencies as high as 500 Hz. This is more than enough to contain the 200 Hz bandwidths of the SIM electronics, and from previous experience, the expected bandwidths of optical fluctuations. NASA one per second time code is also digitized and used primarily as a bookkeeping device. The digital tape contains information in binary coded decimal format and is ready for computer processing.

Processing is done on an IBM system 360/91 computer through programs written in the Fortran IV language. Under contract to NASA-GSFC, Wolf Research and Development Corporation, Bladensburg, Maryland, is responsible for preparation, debugging, and operation of programs to analyze the data. The following description of data analysis concentrates not on specific program instructions but rather on the method of statistical analysis. This method, used over the past two years to analyze horizontal laser scintillation and GEOS-II laser detection scintillation data, was first developed using a small general purpose computer in the Optical Systems Branch. The method is best examined by following a sample data run.

The first information input to the computer for each data track is a series of samples of the positive, zero, and negative calibration voltages v_1, v_2, and v_3. As mentioned previously, $v_1 = +6.0$ volts, $v_2 = 0.0$ volts, and $v_3 = -6.0$ volts. The computer is programmed to determine average values x_1, x_2, and x_3 of the samples for each calibration voltage. A linear relation is assumed to

exist between actual voltage v and sensed value x.

$$v = A(x - B) .$$

Two of the resulting set of three simultaneous equations can be solved for scale (A) and tare (B) factors. This calibration is used later in the data run to assign true voltage readings to the data. It serves to eliminate inevitable gain changes and D.C. offsets present in the recording and reproducing process from magnetic tape. The computer is next presented with samples of the three digit star number. Once again, average values are determined as well as the percentage this average is of positive calibration. This serves to identify the star number. The computer has stored a list of over 100 stars according to their star number, right ascension, and declination. Use of the following information allows calculation of stellar zenith angle and azimuth:

1. Time of data run
2. Sidereal time at Greenwich, England, for zero hours Universal time on the day of observation
3. Stellar coordinates; right ascension and declination
4. Longitude and latitude of observation site.

Data samples then begin to enter the computer. If 20 seconds of data is to be analyzed, the computer will be presented with a series of 20,000 data points for each of the three tracks. All statistics subsequently calculated from the data points will be time averaged over the length of the data run (20 seconds). It is necessary to average data over a time long enough to assure good statistical

accuracy. Estimates based on equivalent bandwidth and resulting number of independent samples suggest at least a ten second averaging time for SIM data. On the other hand, if averaging time is too long, atmospheric or other experimental conditions can change significantly, destroying the meaning of the data. Twenty seconds seems to be a reasonable compromise.

Each data point is assigned a voltage level, v, according to scale and tare factors determined by calibration. Method of analysis then splits into two main directions. In the first direction, the voltage range that includes all the data is divided into a large number, K, of class intervals. The width, Δv, of the class interval, i, may be chosen at will but has as its effective lower limit voltage resolution of A/D equipment. The following are typical parameter values:

voltage range: 0.0 to 10.0 volts

K = 500

Δv = .02 volts

The computer tabulates the number $n(v_i)$, of occurrences of the data record in each class interval and also the percentage occurrences, $p(v_i)$. This in effect establishes a probability density histogram, $P(v_i)$, representing in digital form the probability density function, $P(v)$.

$$p(v_i) = \frac{n(v_i)}{N} .$$

N = total number of data samples

$$P(v_i) = \frac{p(v_i)}{\Delta v}$$

$$\sum_{i=0}^{K} P(v_i)\,\Delta v = 1 .$$

The cumulative density histogram is related to $P(v_i)$ by:

$$C(v_j) \qquad \sum_{i=1}^{j} P(v_i)\,\Delta v .$$

This represents the total probability for voltage less than or equal to the given voltage, v_j. Probability density and cumulative density are related theoretically by:

$$P(v) \qquad \frac{d\,C(v)}{dv}$$

$$C(v) = \int_{-\infty}^{v} P(v)\,dv .$$

The computed probability density function is used to determine means, variances, and higher moments of the data record.

$$\text{Mean} = \bar{v} = \sum_{i=1}^{N} v_i\,P(v_i)\,\Delta v$$

$$j^{th} \text{ moment about the mean} = \sum_{i=1}^{N} (v_i - \bar{v})^j\,P(v_i)\,\Delta v$$

$$= m^j$$

$j = 2$ is the variance, σ^2. The sample mean and sample moments thus computed are not unique for a given sequence of N data points, since they are determined by choice of voltage interval endpoints and by number of class intervals.

The parameters coefficient of kurtosis, k, and skewness, s, help to characterize the probability density function.

$$k = \frac{m^4}{(m^2)^2} - 3.0$$

$$s = \frac{m^3}{(m^2)^{3/2}}$$

Coefficient of kurtosis relates to the width of the distribution and skewness relates to its symmetry. For a gaussian distribution, both k and s will be zero. Random voltage statistics can best be summarized in one parameter, coefficient of variance.

$$\text{Coefficient of variance} = \frac{(\sigma^2)^{1/2}}{\bar{v}} \qquad (4)$$

This parameter has the form of a percentage modulation. It is the ratio of standard deviation of the fluctuating signal to its average value.

The second main direction of analysis is based on data time series; the succession of data samples maintained in their original positions as a function of time. The basis tool in this analysis is the sample autocorrelation function, $R(\tau)$.

$$R(\tau) = \frac{1}{T-\tau} \int_{0}^{T-\tau} v(t)\,v(t+\tau)\,dt \qquad (5)$$

τ = lag time

T = length of data sample

$v(t)$ = voltage level at time t.

The autocorrelation function for random data describes the general dependence of the values of the data at one time on the values at another time. An estimate of the autocorrelation between values of $v(t)$ at times t and $t + \tau$ is just the product of the two values averaged over the length of data sample. τ is the lag time or separation time. For computer analysis, the discrete representation is used.

$$R(\tau) = R(\ell \Delta t) = \frac{1}{N - \tau} \sum_{i=0}^{N-\tau} v_i' \, v_{i+\ell}'$$

ℓ = lag number = 0, 1, 2, $\cdots$ m

m = maximum lag number

N = total number of samples

Δt = interval between samples

$v_i' = v_i - \bar{v}$ = voltage level for the i^{th} sample minus the average voltage level.

For a good estimate of $R(\tau)$, m should be chosen one tenth of N or less.

TYPICAL PARAMETERS

N = 20,000

m = 200

Δt = 1 millisecond

Although $R(\tau)$ is a useful quantity by itself, it is more useful when applied to an estimate of spectral density, $G(f)$.

$$G(f) = \lim_{\Delta f \to 0} \frac{\sigma^2(f)}{\Delta f}$$

Spectral density can be thought of as voltage variance per unit bandwidth. Proceeding from the time domain, $R(\tau)$, to the frequency domain, $G(f)$, requires the Fourier transform of $R(\tau)$ with respect to τ.

$$G(f) = 4 \int_0^\infty R(\tau) \cos(2\pi f \tau) \, d\tau \qquad (6)$$

In discrete form for computer analysis, this becomes:

$$G(f) = 4\Delta t \sum_{\ell=0}^{m} R(\ell \Delta t) \cos \frac{\pi \ell f}{f_c}$$

f = frequency (Hz)

f_c = 500 Hz = frequency cutoff of data

The equivalent bandwidth or frequency resolution in this analysis is B_e.

$$B_e = \frac{2 f_c}{m}$$

For the previously assumed parameters B_e = 5 Hz. The raw estimate spectral density requires smoothing because the variability of the estimate does not decrease with increased sample size or record length. Smoothing or weighting nonuniformly can be accomplished by multiplication by the Hanning lag window,

MODULATION INDEX DATA ANALYSIS

The modulation index track results in a voltage proportional to the modulus of the optical transfer function for the particular spatial frequency used in data taking. Voltage statistics are appropriate and require only a conversion factor to modulus statistics. Laboratory tests generate a plot of modulus versus modulation index voltage. Modulus is just the depth of modulation of the square wave input to simulate the waveform from the detection of chopped starlight. One hundred percent depth of modulation corresponds to a modulus of 1.0. As the depth of modulation is varied, the analog divider and peak detector respond with a change in voltage. Modulus values obtained from this curve are corrected for the effect of electronic and optical background. This is done with average voltage and average background data obtained from the image intensity track. The average value of defocus voltage serves as the zero reference for modulation index voltage. The variance of modulus is read directly from the calibration curve. Data reduction is incomplete without the time series information provided by autocorrelation function and spectral density. This analysis can be performed directly on modulation index voltage. Secant of stellar zenith angle, azimuth and spatial frequency serve to characterize the data run.

IMAGE MOTION DATA ANALYSIS

The image motion track may be handled entirely in terms of voltage statistics, since optical phase, image motion, and output voltage of the electrical phase comparator enjoy a linear relationship. Image motion in the telescope focal

plane is the result of random deviations or tilts in the angle of arrival of various parts or all of the incoming wavefront. These tilts are actually optical phase differences following a Gaussian distribution. Stellar image motion with respect to reference light image causes a change in the relative electrical phase of waveforms from the two detectors. Suitable laboratory calibration yields a conversion factor in volts per arc second for each spatial frequency. Voltage statistics are thus converted to image motion statistics. The conversion to average image position is meaningless in data reduction, since it is not important to know precisely where the image is but how it fluctuates with respect to a fixed point. The important parameter is image motion variance, σ_m^2. Either this number or rms value, σ_m, is plotted versus secant zenith angle of the star. Numbers on image motion must be multiplied by $\sqrt{2}$ to give total two-dimensional image motion. The measured motion is only the component perpendicular to the chopper disk radius. This analysis assumes isotropic image motion. Spectral densities of image motion can be scaled directly from voltage spectral densities.

At the conclusion of computer analysis of stellar data for a particular night, a data summary sheet is prepared. The following information is tabulated for each data run. In addition, data for different stars is combined to yield plots of $\log_e$ (CIV) versus $\log_e$ [secant (zenith angle)] and phase variance versus secant (zenith angle). A modulation transfer function is plotted for each star observed at four or more spatial frequencies. This places the data in a form suitable for interpretation.

Table 4

General Parameters for Each Data Run

1. Data run number
2. Star name and number
3. Zenith angle
4. Secant (zenith angle)
5. Log_e [secant (zenith angle)]
6. Azimuth
7. Time interval for data run
8. Spatial frequency
9. Aperture diameter

Table 5

Statistical Summary for Each Data Run

INTENSITY TRACK
1. CIV = $\sigma_v/\bar{v}$ = coefficient of irradiance variance
2. σ_χ^2 = log amplitude variance
3. $\bar{v}$ = signal mean
4. $\log_e$ (CIV)
5. $\bar{v}_B$ = background mean
MODULATION INDEX TRACK
1. $\sigma_v/\bar{v}$
2. $\bar{v}$ = signal mean
3. $\bar{v}_D$ = defocus mean
IMAGE MOTION TRACK
1. $\bar{v}$ = signal mean
2. σ_m^2 = motion variance
3. σ_m = motion rms

SECTION IV

DATA INTERPRETATION

BACKGROUND

Data interpretation is extremely important for the SIM experiment. Data points are largely dependent on many experimental parameters such as telescope aperture size, local weather, length of data run, wavelength of light, and stellar zenith angle. It would be a hopeless task to control all parameters in any program of experiments. Thus data taken in this experiment must be examined in light of recorded parameters, theoretical analysis, and experimental work of other researchers. Such an examination must be directed toward useful information. Engineering numbers must be arrived at which serve to characterize the data and predict the performance of other optical systems in the presence of atmospheric turbulence. In particular numbers are required to specify the intensity, blurring, and motion of an image formed in the optical system.

In recent years much theoretical and experimental work has been done on the effect of atmospheric turbulence on optical propagation. To date there is no unified theory applicable to this problem, although several treatments have been partially successful in predicting experimental results. The usual starting point is an approximate solution to the scalar wave equation, although some researchers have appealed directly to two point correlation statistics. All approaches attempt to arrive at expressions for log amplitude and phase of the optical wavefront in a plane perpendicular to the direction of propagation through the turbulent

atmosphere. Since amplitude fluctuations are multiplicative rather than additive, log amplitude is modulated in an additive fashion as is phase. As a consequence of the central limit theorem log amplitude and phase follow a normal or Gaussian distribution. Statistics of log amplitude and phase are means, variances, and structure functions. The latter is a particularly useful way of relating the information. It is the mean square difference of values of the physical quantity at two points separated by a distance, r. Log-amplitude, χ, and phase, ϕ, structure functions are defined as follows.

$$D_\chi(r) = \left\langle \left[\chi(r_1) - \chi(r_2)\right]^2 \right\rangle \tag{8}$$

$$D_\phi(r) = \left\langle \left[\phi(r_1) - \phi(r_2)\right]^2 \right\rangle \tag{9}$$

Together they form the wave structure function.

$$D_\psi(r) = D_\chi(r) + D_\phi(r) \tag{10}$$

Theory relates optical statistics (log amplitude and phase statistics) to the statistics of the intervening atmosphere. For this a certain knowledge of the physics of the turbulent process is needed. Statistics of turbulent mixing of air parcels are given in Reference 14 by the Kolmogorov theory. Different parcels of air are at different temperatures and presumably in a certain subrange of sizes, all energy dissipation is through turbulent mixing. Parcel sizes range from an inner scale, ℓ_0, on the order of millimeters at the earth's surface, to an ill-defined outer scale, tens to hundreds of meters. The important result of this theory is a refractive index structure function, $D_N(r; h)$, expressing the mean

square difference of refractive index.

$$D_N(r; h) = C_N^2(h)\, r^{2/3} \tag{11}$$

$C_N^2(h)$, the refractive index structure constant, is a function of altitude above the earth's surface as well as atmospheric conditions. It is essentially a measure of the strength of turbulence. The turbulent profile, $C_N^2(h)$, versus altitude, appears in all equations derived from the theory. Data provided by Hufnagel (Reference 8) gives the most accurate results to date on average turbulent profile. This data was compiled through a combination of stellar scintillation and meteorological measurements. As seen in Figure 10 the profile decreases quite rapidly from a maximum near ground level. The primary distinguishing feature is a sharp peak near 12 kilometers. This has been attributed to the region of high turbulence at the tropopause.

Rather than proceed with a detailed treatment of solutions to the wave equation and their relation to turbulence spectra, end results will be quoted directly. Only these results which apply to ground based observation of starlight will be presented. Expressions will be arrived at which predict the data to be obtained from SIM measurements of stellar irradiance fluctuation, image size, and image motion.

IRRADIANCE STATISTICS

Irradiance fluctuations have been treated by Tartarski (Reference 19). He has arrived at an expression for log amplitude variance, σ_χ^2, of starlight. This

is just four times log irradiance variance.

$$\sigma_\ell^2 = .56\, k^{7/6} (\sec\theta)^{11/6} \int_0^\infty C_N^2(h)\, h^{5/6}\, dh \qquad (12)$$

h = altitude

θ = zenith angle

$k \equiv 2\pi/\lambda$ = wave number

$C_N^2(h)$ = refractive index structure constant

This expression reveals the dependence of scintillation of wavelength, zenith angle, and strength of turbulence. Wavelength dependence is weak and in the visible spectrum amounts to only a small correction factor. In the SIM the optical bandpass is approximately .1 microns. For purposes of scintillation this can be considered monochromatic. On the other hand zenith angle dependence is quite strong. It expresses the relation of scintillation to the amount of air starlight must traverse in order to reach the telescope. Air mass is proportional to secant (zenith angle). Dependence on turbulence is expressed by the integral over turbulent profile, $C_N^2(h)$.

Log amplitude variance is just the statistical parameter computed from SIM intensity output. It is the variance of natural log of the ratio of instantaneous intensity in the stellar image to mean intensity. The other useful statistical parameter is CIV, coefficient of irradiance variance. A straightforward

statistical analysis relates CIV to log amplitude variance.

$$\text{irradiance} \quad I = \langle I \rangle \exp(2\ell)$$

$$\text{log amplitude} = \ell = \frac{1}{2} \log_e I / \langle I \rangle$$

$$\text{irradiance variance} = \sigma_I^2 = \left\langle \left(I - \langle I \rangle \right)^2 \right\rangle$$

$$\text{log amplitude variance} = \sigma_\ell^2 = \left\langle \left(\ell - \langle \ell \rangle \right)^2 \right\rangle$$

$$\sigma_I^2 = \left\langle \left(\langle I \rangle \exp(2\ell) - \langle \langle I \rangle \exp(2\ell) \rangle \right)^2 \right\rangle$$

$$= \langle I \rangle^2 \left\langle \left(\exp(2\ell) - \langle \exp(2\ell) \rangle \right)^2 \right\rangle$$

Since ℓ is a gaussian random variable

$$\langle \exp(2\ell) \rangle = \exp\left[2\langle \ell \rangle + \frac{1}{2} (2)^2 \left\langle \left(\ell - \langle \ell \rangle \right)^2 \right\rangle \right]$$

$$= \exp\left[2\langle \ell \rangle + 2\left\langle \left(\ell - \langle \ell \rangle \right)^2 \right\rangle \right]$$

$$= \exp\left[2\langle \ell \rangle + 2\sigma_\ell^2 \right]$$

but

$$\sigma_\ell = -\langle \ell \rangle$$

$$\therefore \langle \exp(2\ell) \rangle = 1$$

$$\therefore \sigma_I^2 = \langle I \rangle^2 \left\langle \left[\exp(2\ell) - 1 \right]^2 \right\rangle$$

$$= \langle I \rangle^2 \left\langle \exp(4\ell) - 2\exp(2\ell) + 1 \right\rangle$$

$$\langle \exp(2\ell) \rangle = 1$$

$$\langle \exp(4\ell) \rangle = \exp\left[4\langle \ell \rangle + 8\sigma_\ell^2 \right]$$

$$= \exp\left[4\sigma_\ell^2 \right]$$

$$\therefore \sigma_I^2 = \langle I \rangle^2 \left[\exp\left(4\sigma_\ell^2\right) - 1\right]$$

but:

$$CIV^2 = \sigma_I^2 / \langle I \rangle^2$$

$$\therefore \boxed{CIV^2 = \exp\left(4\sigma_\ell^2\right) - 1} \qquad (13)$$

In actual experimental situations use of the above equation is questionable for values of σ_ℓ^2 greater than .1. However, stellar scintillation recorded with a six inch telescope rarely exceeds a value for σ_ℓ^2 of .05, and the equation may be used safely. Furthermore for these smaller values an approximation to this equation can be employed.

$$CIV^2 = \exp\left(4\sigma_\ell^2\right) - 1$$

$$CIV^2 + 1 = \exp\left(4\sigma_\ell^2\right)$$

$$\ell n\left(CIV^2 + 1\right) = 4\sigma_\ell^2$$

$$\ell n\left(CIV^2 + 1\right) = CIV^2 - \frac{CIV^4}{2} + \frac{CIV^6}{3} - \ldots$$

for

$$CIV^2 < 1$$

$$\ell n\left(CIV^2 + 1\right) \approx CIV^2$$

$$\therefore \boxed{CIV^2 \approx 4\sigma_\ell^2} \qquad (14)$$

Tatarski's equation for σ_ℓ^2 pertains to a point detector. The instantaneous irradiance is constant over the entire detector aperture. For larger apertures a reduction in magnitude of scintillation, evidenced by a smaller σ_ℓ^2, is observed.

This effect is attributed to averaging over fluctuations from different areas of the aperture. Both Fried (Reference 4) and Tatarski (Reference 19) predict aperture averaging, which not only reduces scintillation but changes its zenith angle dependence. In this analysis the correlation distance for irradiance fluctuations becomes important.

$$\text{correlation distance} = \sqrt{\lambda H_0 \sec\theta}$$

θ = zenith angle

λ = wavelength

H_0 = scale height of atmosphere

= approximately 15 km.

If telescope diameter, D, is greater than the telescope aperture averaging will take place: while the region $D/\sqrt{\lambda H_0 \sec\theta} \leq 1$ corresponds to little or no averaging. The effect of exceeding the correlation distance has been measured experimentally by Protheroe (Reference 17). He obtained a 2.5 times reduction in CIV in going from a one inch diameter telescope to a six inch diameter. This corresponds to a reduction in σ_ℓ^2 of 6.25. For the six inch diameter telescope, he observed the following dependence on zenith angle.

$$\sigma_\ell^2 \propto \sec^{2.4}\theta$$

$$CIV \propto \sec^{1.2}\theta$$

The calculated correlation distance was around three inches. Protheroe's actual CIV values must be corrected for his experimental technique in order to arrive

at CIV for zenith viewing. When this is done the following average values can be presented: which in turn predict average σ_ℓ^2 values.

Table 6

Average CIV and σ_ℓ^2 Values

	CIV	σ_ℓ^2
Summer	.14	.0049
Winter	.16	.0064

Returning to equation 12 it is noted that the integral over $C_N^2(h)$ includes a factor $h^{5/6}$. Lower altitudes where $C_N^2(h)$ is the largest do not have an important effect on σ_ℓ^2. It is the altitudes where $h^{5/6} C_N^2(h)$ takes on its larger values that figure most prominently in scintillation. There are good practical reasons why scintillation should originate at high altitudes.

(1) The most likely mechanism for generating temperature fluctuations (and thus refractive index fluctuations) is through the combined agencies of wind shear and non-adiabatic lapse rate present at the tropopause, (8 to 14 km). (Reference 13)

(2) Consideration of turbulent element sizes and effective scattering angles show that altitudes of 8 to 14 km are required for the interference patterns known as scintillation to be produced on the ground.

The frequency spectrum of irradiance is determined by the same factors of correlation distance, wavelength, zenith angle, and aperture size. In addition the velocity spectrum of upper altitude winds becomes very important. Increases in

either wavelength, zenith angle, or aperture size are reflected in a decrease in magnitude of scintillation high frequency components. These effects would be observed in spectral densities of stellar image intensity and log amplitude. Tatarski (Reference 19) has developed a theoretical analysis of spectral density parameter dependence.

The physical basis of spectral density aperture dependence can be understood by considering the structure of irradiance in the plane of the telescope aperture. The structure consists of a continuous size spectrum of bright and dark patches changing with respect to time and sweeping across the aperture. As the aperture becomes much larger than the correlation distance the small patches, which have dimensions on the order of correlation distance and are responsible for high frequency components, produce less of an effect due to aperture averaging. Larger patches and therefore lower frequency components do not suffer as much averaging. The rate at which the pattern is swept across the aperture is determined by upper altitude wind profile. Wind velocity is strongly peaked in the 8 to 14 km region of the tropopause, previously asserted to be the region of scintillation origin. This comes as no surprise since turbulence is readily associated with high flow velocities. Typical velocities at the tropopause are from 20 to 100 meters per second and the flow is often referred to as a jet stream. On the basis of the above physical considerations a proportionality to irradiance frequency spectrum can be asserted.

$$f \propto v_n / \sqrt{\lambda H_0 \sec \theta}$$

$\sqrt{\lambda H_0 \sec \zeta}$ = correlation distance

v_n = wind velocity normal to path of propagation

This relation can be used to define a characteristic frequency, f_c, equal to the right hand side above. f_c predicts the maximum frequency of scintillation to be observed if v_n is the maximum wind velocity. f_c can be measured experimentally and then compared with wind speed and zenith angle data.

OPTICAL TRANSFER FUNCTIONS

To analyze atmospheric effects on modulation index or the modulus of the optical transfer functions, it is necessary to return to equation 10 for the wave structure function.

$$D_W(r) = D_\ell(r) + D_\phi(r)$$

Tatarski has related the refractive index structure function, $D_N(r;h)$, from the Kolmogorov theory to the wave structure function and arrived at the following functional dependence.

$$D_W(r) = 2.91\, k^2 r^{5/3} \int_{\text{path of propagation}} C_N^2(z)\, dz$$

For stellar observations the path of propagation, z, should be expressed in terms of altitude, h, and zenith angle, ζ.

$z = h \sec \theta$

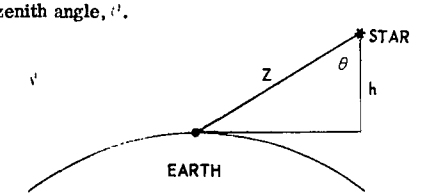

$$\therefore D_W(r) = 2.91\, k^2 r^{5/3} \sec \zeta \int_0^\infty C_N^2(h)\, dh \qquad (15)$$

$k = 2\pi/\lambda$ = wave number

$r = \lambda f$

f = spatial frequency

ζ = zenith angle

h = altitude

Different theoretical approaches by Fried (Reference 6) and Hufnagel and Stanley (Reference 9) have resulted in the same expression for modulus of OTF in terms of the wave structure function,

$$\langle M_{os}(f)\rangle_{short} = M_L(f) \exp\left\{-11.6\pi^2 \lambda^{-1/3} f^{5/3} \sec\theta \int_0^\infty C_N^2(h)\, dh \left[1 - \epsilon\left(\frac{\lambda f}{D}\right)^{1/3}\right]\right\}$$

$$= M_L(f) \exp\left\{-D_W(r)\left[1 - \epsilon\left(\frac{\lambda f}{D}\right)^{1/3}\right]\right\} \qquad (16)$$

ϵ = factor dependent on intensity modulation

$\approx 1/2$

The angular brackets represent time averages short with respect to the effective period of atmospheric fluctuations. $M_{os}(f)$, the modulus measured in SIM, is in reality averaged over a time equal to the reciprocal bandwidth of the modulation index electronics (see Appendix B). The bandwidth is 200 Hz; thus the

averaging time is approximately five milliseconds. The raw modulation index data from the SIM electronics is thus a measure of fluctuations in short term blur circle. Computer generated statistics are average, variance, and higher moments of the short term blur and do not include effects of image motion less than 200 Hz. Blur data in the form of a transfer function contains contributions of the telescope optics and the atmosphere. Laboratory test data provides a telescope optics transfer function. This is divided into the measured $M_{os}(f)$ to arrive at the atmospheric contribution.

$$\exp\left\{-D_w(r)\left[1-\epsilon\left(\frac{\lambda f}{D}\right)^{1/3}\right]\right\} = \frac{\langle M_{os}(f)\rangle_{short}}{M_L(f)} = \langle M_A(f)\rangle_{short} \qquad (17)$$

$M_L(f)$ = telescope optics transfer function

For short term blur the atmospheric OTF is not entirely independent of lens parameters. Equation 17 reveals a dependence on lens diameter. However, the effect of lens aberrations are removed by the division of transfer functions.

Functional dependence in Equation 16 involves wavelength, zenith angle, and strength of turbulence, although the specific form is different than that for irradiance statistics. Modulus dependence on each parameter can be verified experimentally by holding constant all but the parameter under test. The strength of turbulence factor now is an integral over only the refractive index structure constant. For irradiance the integral was the 5/6 ths moment of $C_N^2(h)$ with altitude. Comparison of measured results of the two integrals can result in a crude knowledge of the vertical profile of turbulence; i.e., the dependence of $C_N^2(h)$ on h.

The atmospheric modulus can be written, $\exp\left\{-cf^{5/3}\left[1-\epsilon(\lambda f/D)^{1/3}\right]\right\}$ where f is spatial frequency in cycles per arc second and C is a factor containing the parameter dependence. This predicts the shape of atmospheric OTF. For spatial frequencies much less than the resolution cutoff, D/λ the shape is controlled by the factor, $\exp\left(-cf^{5/3}\right)$. As the resolution cutoff is approached the factor $\exp\left[c\epsilon\left(\lambda f^5/D\right)^{1/3}\right]$ becomes dominant. Using the expression $\exp\left(-cf^{5/3}\right)$ the dependence of image profile on the parameters contained in C can be derived. The two-dimensional Fourier transform result derived in Appendix A provides the necessary relation.

$$I(s) = 2\int_0^\infty \omega M(\omega) J_0(2\pi s\omega)\, d\omega$$

ω = spatial frequency (cycles/arc second)

s = arc seconds

Now, substitute in:

$$M(\omega) = \exp\left(-c\omega^{5/3}\right)$$

$$\therefore I(s) = 2\int_0^\infty \omega \exp\left(-c\omega^{5/3}\right) J_0(2\pi s\omega)\, d\omega$$

$$\approx 2\int_0^\infty \omega \exp\left(-c\omega^2\right) J_0(2\pi s\omega)\, d\omega$$

$$= \frac{1}{c}\exp\left(-\frac{s^2}{c/\pi^2}\right)$$

This is a gaussian shape with variance σ_s^2.

$$\sigma_s^2 = \frac{c}{2\pi^2}$$

or

$$\sigma_s^2 = 5.8\ \lambda^{-1/3} \sec\theta \int_0^\infty C_N^2(h)\, dh$$

$$\sigma_s = 2.4\ \lambda^{-1/6} (\sec\theta)^{1/2} \left[\int_0^\infty C_N^2(h)\, dh\right]^{1/2}$$

σ_s is the rms value of $I(s)$, i.e. the rms of image size. It is seen to be proportional to the negative sixth root of wavelength, the square root of zenith angle and the square root of integrated turbulence.

Rather than image profile a specification of optical resolution, R, through the atmosphere can be made.

$$R = \int_0^\infty \frac{\langle M_{os}(f)\rangle_{short}}{M_L(f)}\, df \qquad (18)$$

Resolution is just the area under the OTF curve. It is equivalent to the Strehl definition of image quality.

IMAGE MOTION

Fluctuations in the position of image center of gravity result from atmospherically induced changes in the phase or shape of the incoming wavefront. Most changes (90%) can be attributed to random linear phase shifts or tilts in the wavefront. Tilts cause image displacement. The other principal wavefront degradation is quadratic in form and leads to focusing errors; thus contributing to blurring of the image. Tatarski (Reference 19) has related wavefront tilts to phase structure function by examining a two point correlation or interferometer experiment (Figure 11).

Consider two point detectors A and B separated by a distance d. Incoming light represented by a wavefront tilted with respect to d is brought to a focus after passing through the point detectors. The angle of tilt, $\Delta\alpha$, radians, is equal to the angular displacement of image in the focal plane. The phase shift, $\Delta\phi$, between A and B can be expressed in terms of tilt angle.

$$\Delta\phi = \phi_B - \phi_A = kd\,\Delta\alpha$$

The mean square difference of phase is just the definition of phase structure function.

$$\langle(\Delta\phi)^2\rangle = \langle(\phi_B - \phi_A)^2\rangle = D_\phi(d)$$

$$= k^2 d^2 \langle(\Delta\alpha)^2\rangle$$

$$\therefore \langle(\Delta\alpha)^2\rangle = \frac{D_\phi(d)}{k^2 d^2} \qquad (19)$$

< > = ensemble average

Tatarski employs his expression for phase structure function based on the Rytov approximation to the wave equation and the Kolmogorov turbulence spectrum.

$$D_\phi(d) = K k^2 d^{5/3} \int_0^\infty C_N^2(z)\, dz$$

K = a constant

For stellar observations this becomes:

$$D_\phi(d) = K k^2 d^{5/3} \sec\theta \int_0^\infty C_N^2(h)\, dh$$

Substitution in Equation 19 leads to an expression for mean square angular fluctuations.

$$\langle(\Delta\alpha)^2\rangle = K d^{-1/3} \sec\theta \int_0^\infty C_N^2(h)\, dh \qquad (20)$$

In the SIM experiment light reception is through one fairly large circular aperture. In generalizing to such cases from the interferometer result above, Tatarski asserts that aperture diameter plays the role of point detector separation, d; with the only other change being in the value of proportionality constant, K. The resulting equation:

$$\langle(\Delta\alpha)^2_{TEL}\rangle = K' D^{-1/3} \sec\theta \int_0^\infty C_N^2(h)\, dh \qquad (21)$$

- σ_s^2, image motion variance measured by SIM

is a starting point for the usual tests of parameter dependence. Strangely enough Equation 21 predicts that image motion is independent of wavelength and has only a weak aperture dependence $D^{-1/3}$, for apertures greater than the inner scale of turbulence (a few millimeters). The table below lists aperture dependence for various diameters.

Table 7

Image Motion Aperture Dependence

Aperture Diameter		$D^{-1/3}$
(inches)	(cm)	($cm^{-1/3}$)
1	2.54	.787
3	7.62	.509
6	15.2	.404
12	30.5	.320
60	152	.188

Based on this analysis variance of image motion present in a six inch diameter telescope would be reduced only by a factor of about two for a sixty inch diameter telescope. Image motion may be a factor of concern in even the larger telescopes.

Image motion dependence on turbulence is expressed by the integral over $C_N^2(h)$. The integral appears in the same form as that for the modulus of the optical transfer function. Since $C_N^2(h)$ appears alone in the integral, turbulence strength at each altitude is weighed equally. Lower altitudes where $C_N^2(h)$ takes on its largest values contribute most heavily to the integral. Due to the sensitivity

of image motion and size data to local lower atmospheric conditions, experimental results of various researchers are difficult to compare accurately. Quoted below are average nighttime results reported by Hosfeld (Reference 7) and Johnson et al. (Reference 12). These may be used for general comparison.

Table 8

Average Image Size and Motion

	Rms Motion (Arc Seconds)	Rms Size (Arc Seconds)
Hosfeld	.62	1.3
Johnson et al.	.34	---

References 9 and 10 detail the analysis of image motion in terms of a transfer function $\langle M_m(f)\rangle_{long}$. The formula arrived at:

$$\langle M_m(f)\rangle_{long} = \exp\left(-4\pi^2 f^2 \sigma_s^2\right) \tag{22}$$

f = spatial frequency (arc seconds)

σ_s^2 = one-dimensional image motion variance

is a good approximation, but not rigorously correct. If short term blur and image motion are assumed uncorrelated, they can be simply combined to yield an expression for the long term blur.

$$\langle M_A(f)\rangle_{long} = \langle M_A(f)\rangle_{short} \langle M_m(f)\rangle_{long} \tag{23}$$

This is the OTF to be expected when the measurement is made over a long time or the telescope has an extremely large aperture; hence little image motion.

Fourier inversion of $\langle M_A(f)\rangle_{long}$ leads to long term image profile; including all the effects of blur and movement. This is the quantity proportional to optical heterodyne S/N (Reference 5).

SECTION V

LABORATORY AND FIELD TESTS

ELECTRONIC TESTS

Prior to deployment of the Stellar Image Monitor Experiment in the field, a series of laboratory tests and calibration runs were performed. The first system component to be tested was the electronic pre-processing system. Figures 12 and 13 are measured frequency and phase response of the bandpass and lowpass filter sections. Bandwidths are 3100 Hz ± 200 Hz and 200 Hz, respectively. Frequency response was measured by using a sine wave signal generator in place of inputs from photomultiplier and photodiode. Phase response was measured on an oscilloscope. Filter input and output were applied to the vertical deflection and horizontal sweep respectively. The resulting lissajous pattern displayed on a phase reticle gave readings of phase difference. Gain and linearity tests of the amplifiers were also performed. This served to calibrate the image intensity track.

Modulation index calibration required a measure of combined response of analog divider and peak detector. Sine waves at the chopping frequency were input in place of signals from the photomultiplier. Modulation index (peak A.C. divided by D.C.) of this input was measured at the input terminals of the analog

divider. Measured values of peak detector output voltage for the given modulation index or % modulation are shown in Figure 14. This curve applies for D.C. voltage in the range -1.0 to -3.0 volts. It should be noted that linearity is not an important consideration in this output since the expected fluctuations will be small compared to their average value. Percent modulation determined from this curve must be multiplied by

$$\frac{\text{D.C. + BGND}}{\text{D.C.}} \left(\frac{\text{D.C. GAIN}}{\text{A.C. GAIN}}\right)$$

to correct for filter gains and any D.C. offset voltage. The symbol BGND, or background, represents this offset. D.C. + BGND information is available from the image intensity track. Filter gains were measured during calibration and their ratio is:

$$\frac{\text{D.C. GAIN}}{\text{A.C. GAIN}} = 1.025$$

OPTICAL TESTS

Calibration and testing of the image motion electronics employed an artificial star source, Figure 15. A point source at the focus of an f/10 twenty inch diameter collimating mirror represented the small angular size and parallel light of a star. The point source was either white light or .6328 micron red light from a Spectra Physics 131 helium-neon laser. Light from an incandescent lamp filament focused on a variable size pinhole served as the white light point source. In both cases a further reduction in spot size was achieved through microscope objectives. Source sizes were determined as follows.

White Light

$$\frac{\text{Pinhole Diameter}}{\text{Microscope Objective Power}} \quad \text{Source Diameter, d}$$

Red Light

$$\left(\begin{matrix}\text{Effective Focal Length}\\ \text{of Microscope Objective}\end{matrix}\right)\left(\begin{matrix}\text{Laser}\\ \text{Divergence}\end{matrix}\right) = \text{Source Diameter, d}$$

The scale factor from linear to angular measure in the focal plane of the twenty inch collimator is calculated as follows.

$$\frac{\text{Source Size}}{\text{Arc Second}} = \left(\frac{\text{Collimator}}{\text{Focal Length}}\right)\left(\frac{\text{Radians}}{\text{Arc Second}}\right)$$

$$\frac{\text{d}}{\text{Arc Second}} = (200 \text{ Inches})\left(4.85 \times 10^{-6} \frac{\text{Radians}}{\text{Arc Second}}\right)$$

$$= .00097 \frac{\text{Inches}}{\text{Arc Second}}$$

$$\approx .001 \frac{\text{Inches}}{\text{Arc Second}}$$

Therefore each thousandth of an inch in the focal plane corresponds to one arc second. Source sizes were kept smaller than the theoretical angular resolution of six inch diameter optics.

Collimated light produced by this test set-up was allowed to enter the six inch diameter optics of the Stellar Image Monitor after traversing about 40 feet of laboratory air space. The point sources were mounted on an optical bench equipped with a translation slide. Movement of the point source in increments of .001 inch in the focal plane could be measured there and produced the corresponding number of arc seconds deviation. The D.C. voltage output of the SIM

phase comparator was recorded as a function of this arc second displacement. The output of the phase comparator was not a pure D.C. voltage but contained frequency components due to room vibration, air path turbulence, and chopper pattern centering error. The resultant plot, Figure 16, yields the desired calibration factor in volts per arc second. This factor depends linearly on spatial frequency. For the spatial frequency used in the calibration the rms error was approximately .1 arc second. It should be noted that the calibration curve is cyclic with a linear response in the mid range of voltages. Thus in actual data recording the average value of phase comparator output should be maintained at approximately 3.5 volts. A check on spatial frequency was made by noting the number of cycles of the response curve per arc second. The results agreed with microscope objective power being used and theoretical spot size calculations.

Using the artificial star system described above optical transfer functions for the SIM in white light and red light were generated (Figure 17). This was done by varying microscope objective power in the SIM. Measured OTF shows a degradation of performance in white light while monochromatic red light performance is close to the diffraction limit.[1] Chromatic aberration causing this effect must be present in the SIM optics since the collimating system is reflective.

[1]See Appendix A for OTF of a diffraction limited optical system with six inch diameter circular aperture.

FIELD TESTS AND DATA

All field tests to date have been conducted at the Goddard Optical Research Facility located approximately 4.5 miles from GSFC in an open field. The SIM was placed on a 12 inch high concrete slab approximately 15 feet from a 20 by 20 foot trailer. This building supplied the necessary power and support capability. Time and reference signals were available from an Astrodata time code generator located in an adjacent building. The telescope mount was roughly aligned in the North-South direction. Standards alignment procedures were followed to set the polar axis for the latitude of 39 degrees 1 minute and to make fine adjustments in North-South pointing. Data runs were taken on various clear evenings during fall-winter 1968-1969. Of the data analyzed by computer, representative statistical records are presented here.

Figure 18 contains chart recordings of the three tracks of the SIM for data run 118. Experimental parameters that characterize the data run are listed beside the chart recordings. Timing marks at one second intervals are located along the top. Appropriate calibrations are indicated for the vertical scale on each recording. The modulation index track has indications of percent modulation and the image motion track is calibrated in arc seconds. The computer generated statistical record is presented in table 9. The three salient results are:

log amplitude variance = .018

OTF modulus = .78

image motion variance = .18 (Arc Seconds)^2

Table 9

Statistics for Data Run 118

GENERAL PARAMETERS:

1. DATA RUN 118
2. STAR: ALDEBARAN NO. 168
3. ZENITH ANGLE (ZA) = 29.7°
4. SEC (ZA) = 1.15
5. LOG_e [SEC (ZA)] = .141
6. AZIMUTH = 112°
7. 20 SECOND DATA RECORD: 301-08-46-36→56
8. SPATIAL FREQUENCY = .047 CYCLES/ARC SECOND
9. APERTURE DIAMETER = 6 INCHES

STATISTICAL SUMMARY:

INTENSITY TRACK
1. CIV = .26
2. σ_ℓ^2 = .018
3. $\bar{v}$ = 2.84 VOLTS
4. LOG_e (CIV) = -1.34
5. $\bar{v}_B$ = .40 VOLTS

MODULATION INDEX TRACK
1. $\sigma_v / \bar{v}$ = .05
2. $\bar{v}$ = 3.9 VOLTS
3. $\bar{v}_D$ = .47 VOLTS

IMAGE MOTION TRACK
1. $\bar{v}$ = 4.2 VOLTS
2. σ_m^2 = .18 (ARC SECONDS)^2
3. σ_m = .43 ARC SECONDS

Figures 18 through 26 summarize data taken during the following nights.

Table 10

Dates of Stellar Observations

Night	Date (Zulu)	Local
269	25 SEP 68	24 SEP 68
292	8 OCT 68	7 OCT 68
301	17 OCT 68	16 OCT 68
324	19 NOV 68	18 NOV 68

Included here are statistics for 58 data runs. This amounts to an analysis of over 110,000 data points.

In Figure 19 irradiance statistics are presented in a plot of $\log_e$ (CIV) versus $\log_e$ [secant (zenith angle)]. All data was taken with a six inch aperture. Protheroe's experimentally observed zenith angle dependence is plotted as a straight line through the data points. There is good agreement with this dependence for zenith angles less than 60 degrees. For larger zenith angles the effect of stellar azimuth becomes important and data scatter is evident. Vertical axis intercepts yield the values of CIV for zenith viewing; 11% and 21% respectively on the two nights. These values compare with Protheroe's average values of 14% and 16% for a six inch aperture. CIV may be converted to log amplitude variance, σ_ℓ^2, using the approximation:

$$CIV^2 \approx 4\sigma_\ell^2$$

Spectral densities of irradiance are shown in Figures 20, 22, and 23. The importance of upper altitude wind velocity is dramatically demonstrated by Figure 20 and the accompanying wind profiles (Figure 21) for each day. Wind profile for the Washington, D.C. vicinity is measured twice daily by balloon flights and is available from the National Weather Record Center, Asheville, North Carolina. The wind data presented was taken at 6:15 p.m. on the day of each series of stellar observations. On day 269 maximum wind velocity at the tropopause was unusually low (approximately ten meters/second), resulting in a sharp reduction in scintillation frequency content. On the other hand maximum wind velocity on day 301 was five times as great. Measured scintillation frequency content showed a corresponding increase of a factor of five for this day. The frequency, f_B, at which normalized spectral density of scintillation is down to one twentieth of its zero frequency value can be used as a measure of bandwidth. Data presented in Table 11 for f_B and maximum wind velocity reveal almost a linear dependence

Table 11

Scintillation Bandwidth Dependence on Wind Velocity

Night	f_B (Hz)	Maximum Wind Velocity (meters/second)	Altitude (kilometers)
269	35	10	13
292	80	21	13
301	142	49	10

of bandwidth on wind velocity. Scintillation data was taken with a six inch aperture and at approximately the same zenith angle.

The zenith angle dependence of frequency content is presented in Figure 22. Data was taken for two stars with the same aperture: Capella, near the horizon and other, Deneb, near zenith. Bandwidth, f_B, for these two data runs taken only nine minutes apart reveal a square root of secant (zenith angle) relationship predicted by theory. Finally the aperture dependence of frequency content is demonstrated in Figure 23. Data was taken for the star Capella with apertures of six inches and one inch. Data runs were taken only 21 minutes apart thus effectively removing any confusion due to changing zenith angle or wind velocity. Bandwidth reduction is a factor of 2 for the larger aperture. CIV values measured with the one inch and six inch aperture were .39 and .24 respectively. This agrees well with Protheroe's measured reduction of a factor of 2.5.

Optical transfer functions were measured for the stars Sirius (zenith angle = 70°) and Capella (zenith angle = 50°) on November 18, 1968. These are plotted in Figure 24 along with the predicted OTF (Equation 17) using Hufnagel's average turbulent profile data (Figure 10). Average image profiles were constructed for each OTF by the two-dimensional spatial Fourier transform technique described in Appendix A. The results plotted in Figure 25 are characterized by an rms image blur circle. This is a measure of image profile radius. Rms values exhibit the expected zenith angle dependence.

Representative image motion data is presented in Figure 26 for night 292 and includes observations over several hours for stars in all parts of the night sky. The plot of rms image motion versus secant (zenith angle) includes the theoretical square root of zenith angle drawn through the value of image motion at zenith. Data agrees well with this dependence, although data scatter increases for large zenith angles. Spectral densities of image motion, Figure 27, reveal that essentially all motion is confined to a bandwidth of 30 Hz. This contrasts with bandwidths of 200 Hz or more for irradiance fluctuations. Further reduction is apparent in frequency content for large zenith angles compared to zenith viewing. Comparison of image motion and profile data with that obtained by other researches is risky at best. However, data of Hosfeld and Johnson et al. can be used for order of magnitude comparison.

REFERENCES

1. Born, M. and Wolf, E.: Principles of Optics. Pergamon Press (New York), 1959.

2. Coulman, C. E.: Dependence of Image Quality on Horizontal Range in a Turbulent Atmosphere. J. Optical Soc. Am., Vol. 56, No. 9, Sept. 1966, pp. 1232-1238.

3. Coulman, C. E.: Optical Image Quality in a Turbulent Atmosphere. J. Optical Soc. Am., Vol. 55, No. 7, July 1965, pp. 806-812.

4. Fried, D. L.: Aperture Averaging of Scintillation. J. Optical Soc. Am., Vol. 57, No. 2, February 1967, pp. 169-174.

5. Fried, D. L.: Optical Heterodyne Detection of an Atmospherically Distorted Signal Wavefront. Proc. IEEE, Vol. 55, No. 1, Jan. 1967, pp. 127-137.

6. Fried, D. L.: Optical Resolution Through a Randomly Inhomogeneous Medium for Very Long and Very Short Exposures. J. Optical Soc. Am., Vol. 56, No. 10, Oct. 1966, pp. 1372-1379.

7. Hosfeld, Roger: Measurements of Size of Stellar Images. Joint Scientific Report 2 (AFCRC-TN-55-873, ASTIA No. AD 83215), Physics and Astronomy Dept. Ohio State Univ., June 1955.

8. Hufnagel, R. E.: An Improved Model Turbulent Atmosphere. Appendix 3 (Restoration of Atmospherically Degraded Images, Vol. 2), Woods Hole Summer Study, July 1966.

9. Hufnagel, R. E.: On the Mean Short Term Blur. Appendix 4 (Restoration of Atmospherically Degraded Images, Vol. 2), Woods Hole Summer Study, July 1966.

10. Hufnagel, R. E.: Understanding the Physics of Seeing through Turbulent Atmospheres. Paper presented at local SPIE mtg. (Patrick A. F. Base, Florida), Nov. 1963.

11. Hufnagel, R. E. and Stanley, N. R.: Modulation Transfer Function Associated with Image Transmission through a Turbulent Media, J. Optical Soc. Am., Vol. 54, No. 1, Jan. 1964, pp. 52-61.

12. Johnson, H. L. Gardiner, A. J., Gifford, F., Mitchell, R. I., Giclas, H. L., Wilson, A. G.: Optical Studies of Atmospheric Turbulence. Final Report (AFCRC-TR-56-261, ASTIA No. AD 96354), Lowell Observatory, Flagstaff, Arizona, 1956.

13. Keller, G. Protheroe, W. M., Barnhart, P. E., Galli, J.: Investigations of Stellar Scintillation and the Behavior of Telescope Images. Final Report (AFCRC-TR-186, ASTIA No. AD 117279), Physics and Astronomy Dept., Ohio State Univ., December 1956.

14. Kolmogorov, A. N.: Dissipation of Energy in Locally Isotropic Turbulence. (Doklady Akad. Nauk SSSR), Vol. 32, 1941.

15. Lindberg, P. J.: Measurement of Contrast Transmission Characteristics in Optical Image Formation. Opt. Acta, Vol. 2, Sept. 1954, pp. 80-89.

16. Linfoot, E. H.: Fourier Methods in Optical Image Evaluation. Focal Press (London), 1964.

17. Protheroe, W. M.: Preliminary Report on Stellar Scintillation. Scientific Report 4 (AF 19 (604) - 41, ASTIA No. AD 56040), Physics and Astronomy Dept., Ohio State Univ., Nov. 1954.

18. Ramsay, J. V. and Kobler, H.: A Stellar Image Monitor. Observatory, Vol. 82, June 1962, pp. 107-111.

19. Tatarski, V. I. (R. A. Silverman, Trans.): Wave Propagation in a Turbulent Medium. McGraw-Hill Book Co., Inc., 1961.

APPENDIX A

IMAGE INTENSITY PROFILE AND OPTICAL TRANSFER FUNCTION

The diffraction image formed in an optical system is characterized by a normalized intensity distribution called the optical spread function, S.

$$S = S(x, y; x', y'; \lambda) = S(\vec{x}, \vec{x}'; \lambda) \tag{A1}$$

(light flux in $(\lambda + d\lambda)$ which originates in $d\vec{x}'$ and passes through the optics to fall on $d\vec{x}$, divided by $d\vec{x}\, d\vec{x}'\, d\lambda$)

$\vec{x}'$ = two dimensional vector in object plane

$\vec{x}$ = two dimensional vector in image plane

The optical spread function is assumed to be time independent and normalized such that:

$$\int_{-\infty}^{\infty} S(\vec{x}; \vec{x}'; \lambda)\, d\vec{x} = 1$$

Use of a transfer function to describe the optical system requires the existence of an isoplanatism patch, area in the object field over which wave aberrations are effectively constant. This enables the optical spread function to be written:

$$S = S(\vec{x} - \vec{x}'; \lambda) \tag{A2}$$

The optical transfer function, $T(\vec{f})$, is defined as the Fourier transform of S. The transform variable is $\vec{f}$, two-dimensional spatial frequency.

$$T(\vec{f}) \quad \int_{-\infty}^{\infty} S(\vec{x} - \vec{x}'; \lambda) \exp\left[-2\pi i\, \vec{f} \cdot (\vec{x} - \vec{x}')\right] d\vec{x} \tag{A3}$$

$$S(\vec{x} - \vec{x}'; \lambda) = \int_{-\infty}^{\infty} T(\vec{f}) \exp\left[2\pi i\, \vec{f} \cdot (\vec{x} - \vec{x}')\right] d\vec{f} \tag{A4}$$

The object intensity distribution, $O(\vec{x}')$ can be written in terms of a Fourier integral of spatial frequencies (Reference 16).

$$O(\vec{x}') = \int_{-\infty}^{\infty} W(\vec{f}) \exp(2\pi i\, \vec{f} \cdot \vec{x}')\, df \tag{A5}$$

$$W(\vec{f}) = \int_{-\infty}^{\infty} O(\vec{x}') \exp(-2\pi i\, \vec{f} \cdot \vec{x}')\, d\vec{x}' \tag{A6}$$

$W(\vec{f})$ = Fourier transform of $O(\vec{x}')$

Image intensity distribution, $I(\vec{x})$, is by definition of the optical spread function, just the convolution of $S(\vec{x} - \vec{x}'; \lambda)$ with $O(\vec{x}')$.

$$I(\vec{x}) = \int_{-\infty}^{\infty} S(\vec{x} - \vec{x}'; \lambda)\, O(\vec{x}')\, d\vec{x}' \tag{A7}$$

Equation A4 for S and Equation A7 for I allow image intensity to be expressed in terms of the transfer function.

$$I(\vec{x}) = \int_{-\infty}^{\infty} S(\vec{x} - \vec{x}'; \lambda)\, O(\vec{x}')\, d\vec{x}' \tag{A8}$$

$$= \iint_{-\infty}^{\infty} T(\vec{f}) \exp\left[2\pi i\, \vec{f} \cdot (\vec{x} - \vec{x}')\right] d\vec{f}\, O(\vec{x}')\, d\vec{x}'$$

$$= \iint_{-\infty}^{\infty} T(\vec{f}) \exp\left[2\pi i\, \vec{f} \cdot (\vec{x} - \vec{x}')\right] O(\vec{x}')\, d\vec{x}'\, d\vec{f}$$

$$= \int_{-\infty}^{\infty} T(\vec{f}) \exp(2\pi i\, \vec{f} \cdot \vec{x}) \int_{-\infty}^{\infty} O(\vec{x}') \exp(-2\pi i\, \vec{f} \cdot \vec{x}')\, d\vec{x}'\, d\vec{f}$$

$$= \int_{-\infty}^{\infty} T(\vec{f}) \exp(2\pi i\, \vec{f} \cdot \vec{x})\, W(\vec{f})\, d\vec{f} \tag{A9}$$

If the object is a point source, $O(\vec{x}') = \delta(\vec{x}')$

$$W(\vec{f}) = \int_{-\infty}^{\infty} \delta(\vec{x}') \exp(-2\pi i\, \vec{f} \cdot \vec{x}')\, d\vec{x}' = 1$$

$$\therefore I(\vec{x}) = \int_{-\infty}^{\infty} T(\vec{f}) \exp(2\pi i\, \vec{f} \cdot \vec{x})\, d\vec{f} \tag{A10}$$

$T(\vec{f})$ is in general complex and can be written in terms of a modulus and complex argument.

$$T(\vec{f}) = M(\vec{f}) \exp\left[2\pi i\, \phi(\vec{f})\right]$$

For real symmetric images the transfer function is real. $T(\vec{f}) = M(\vec{f})$

$$I(\vec{x}) = \int_{-\infty}^{\infty} M(\vec{f}) \exp(2\pi i\, \vec{f} \cdot \vec{x})\, d\vec{f} \tag{A11}$$

A transformation to polar coordinates for both $\vec{x}$ and $\vec{f}$ allows I to be expressed in a form more suitable for computation.

$$I(x, y) = \iint_{-\infty}^{\infty} M(f, g) \exp\left[2\pi i\, (fx + gy)\right] df\, dg$$

$$f = \omega \cos\phi \qquad x = r \cos\theta$$

$$g = \omega \sin\phi \qquad y = r \sin\theta$$

$$I(r, \theta) = \int_0^{\infty} \int_0^{2\pi} M(\omega, \phi) \exp\left[2\pi i\, r\, \omega \cos(\phi - \theta)\right] \omega\, d\phi\, d\omega$$

Symmetry arguments require that I be θ independent and M be ϕ independent.

$$I(r) = \int_0^{\infty} M(\omega)\, \omega \int_0^{2\pi} \exp(2\pi i\, r\, \omega \cos\phi)\, d\phi\, d\omega$$

or

$$\boxed{I(r) = \int_0^{\infty} M(\omega)\, \omega J_0(2\pi r \omega)\, d\omega} \tag{A12}$$

This is the final form relating image intensity and the transfer function.

The theoretical transfer function for a diffraction limited optical system with circular aperture has been computed. Only the result is quoted here.

$$M(\omega) = \frac{2}{\pi}\left\{\cos^{-1}\frac{\lambda}{D}\omega - \frac{\lambda\omega}{D}\left[1-\left(\frac{\lambda\omega}{D}\right)^2\right]^{1/2}\right\} \qquad \text{(A13)}$$

λ = wavelength

D = aperture diameter

ω = spatial frequency in cycles per arc second.

Substitution of this expression into Equation (A12) yields the familiar Airy pattern for a diffraction limited lens.

$$\frac{I(r)}{I_0} = \left[\frac{2J_1(\pi Dr/\lambda F)}{\pi Dr/\lambda F}\right]^2$$

F = system focal length

In angular measure this becomes:

$$\frac{I(S)}{I_0} = \left[\frac{2J_1\left(\frac{\pi DS}{\lambda}\right)}{\frac{\pi DS}{\lambda}}\right]^2 \qquad \text{(A14)}$$

S = arc seconds

This expression is plotted in Figure 25.

APPENDIX B

WAVEFORM ANALYSIS

Electrical signals generated by the detector package of the SIM are amplitude and frequency modulated by atmospheric optical effects. The electronic pre-processing system separately determines the effects on signal modulation of changes in stellar image intensity, size, and position. A clearer understanding of this process can be achieved by modeling the atmospheric effects with single frequency sinusoidal components. The chopping of the stellar image is a further modulation that must be considered. The voltage, from the photomultiplier tube is represented by:

$$V(t) \quad V_0\left[\frac{1}{2} + \frac{m_0}{2}\cos(\omega_c t + \phi)\right]$$

V_0 = voltage magnitude

$V_0/2$ = D.C. level

$V_0 m_0/2$ = magnitude of chopping frequency component

ω_c = chopping frequency = 3.1 KHz

ϕ = phase of chopping frequency component

The actual PMT voltage includes, in addition, frequencies at integral multiples of the fundamental, ω_c. These are beyond the frequency range of interest and will be ignored here. The voltage magnitude, V_0, is intensity modulated by image intensity variations, assumed for this analysis to be at the single

frequency, ω_A.

$$\omega_A \leq 200 \text{ Hz} .$$

$$V_0 = \left(1 - m_A \cos \omega_A t\right)$$

m_A = depth of intensity modulation

Variation in image size do not affect the D.C. value of the waveform but cause an intensity modulation of the magnitude of the chopping frequency component, $v_0 m_0/2$.

$$m_0 = \left(1 - m_m \cos \omega_m t\right)$$

ω_m = image size modulation frequency

m_m = depth of size modulation

Image position changes are reflected in phase, ϕ, of the chopped waveform. Phase modulation is assumed to be at the single frequency, ω_ϕ.

$$\phi = m_\phi \sin \omega_\phi$$

The PMT output voltage under these models becomes:

$$V(t) = \left(1 - m_A \cos \omega_A t\right)\left[\frac{1}{2} + \left(\frac{1}{2} - \frac{m_m}{2} \cos \omega_m t\right) \cos\left(\omega_c t + m_\phi \sin \omega_\phi t\right)\right]$$

In the electronic preprocessing system $V(t)$ is split two ways. The first way passes through a low pass filter where all signals at or near the chopping frequency are blocked.

The output of the low pass filter,

$$V_L(t) = \left(\frac{1}{2} - \frac{m_A}{2} \cos \omega_A t\right)$$

is just the intensity modulation of the image. The second path is through a band pass filter where all low frequency components are blocked.

$$V_B(t) = \left(1 - m_A \cos \omega_A t\right)\left(\frac{1}{2} - \frac{m_m}{2} \cos \omega_m t\right) \cos\left(\omega_c t + m_\phi \sin \omega_\phi t\right)$$

Both filter outputs are fed into a divider section where the operation

$$V_B(t) \cdot V_L(t) = V_D(t)$$

is performed. This step removes intensity modulation and passes the frequency components due to size and position changes as sidebands about the chopping frequency. The structure of these sidebands can be examined through trigonometric identities.

$$V_D(t) = \left(\frac{1}{2} - \frac{m_m}{2} \cos \omega_m t\right) \cos\left(\omega_c t + m_\phi \sin \omega_\phi t\right)$$

$$= \frac{m_0}{2} \cos\left(\omega_c t + m_\phi \sin \omega_\phi t\right)$$

$$= \frac{m_0}{2} \cos \omega_c t \cos\left(m_\phi \sin \omega_\phi t\right)$$

$$- \frac{m_0}{2} \sin \omega_c t \sin\left(m_\phi \sin \omega_\phi t\right)$$

$$V_D(t) = m_0 \cos \omega_c t \left[J_0(m_\phi) + 2 \sum_{k=1}^{\infty} J_{2k}(m_\phi) \cos(2k \omega_\phi t) \right]$$

$$- m_0 \sin \omega_c t \; 2 \left\{ \sum_{k=0}^{\infty} J_{2k+1}(m_\phi) \sin\left[(2k+1)\omega_\phi t\right] \right\}$$

$$= \frac{m_0}{2} J_0(m_\phi) \cos \omega_c t$$

$$+ \frac{m_0}{2} \sum_{k=1}^{\infty} J_{2k}(m_\phi) \left\{ \cos\left[(\omega_c + 2k\omega_\phi)t\right] + \cos\left[(\omega_c - 2k\omega_\phi)t\right] \right\}$$

$$- \frac{m_0}{2} \sum_{k=2}^{\infty} J_{2k+1}(m_\phi) \left\{ \cos\left[(\omega_c - (2k+1)\omega_\phi)t\right] - \cos\left[(\omega_c + (2k+1)\omega_\phi)t\right] \right\}$$

$$- \frac{m_0}{2} J_0(m_\phi) \cos \omega_c t$$

$$- \frac{m_0}{2} J_1(m_\phi) \left[\cos(\omega_c - \omega_\phi)t - \cos(\omega_c + \omega_\phi)t \right]$$

$$+ \frac{m_0}{2} J_2(m_\phi) \left[\cos(\omega_c - 2\omega_\phi)t + \cos(\omega_c + 2\omega_\phi)t \right]$$

$$- \frac{m_0}{2} J_3(m_\phi) \left[\cos(\omega_c - 3\omega_\phi)t + \cos(\omega_c + 3\omega_\phi)t \right]$$

$$+ \vdots$$

$J_i(m_\phi)$ is the Bessel function of order i and argument, m_ϕ, the depth of modulation of image position. $V_D(t)$ is fed into a peak detector stage where the peak values of frequency components in the passband ±200 Hz around 3 KHz are detected. Image motion at frequencies greater than 200 Hz reduces the peak value,

while the effect of lower frequency image motion is removed by the cancellation of Bessel function terms. Thus the peak value is a measure of image size variations, represented by

$$m_0 = (1 - m_m \cos \omega_m t)$$

from D.C. to 200 Hz and image motion greater than 200 Hz. This corresponds to a measurement of the short term blur circle of the image. Short term is the reciprocal of 200 Hz or 5 milliseconds.

Image motion at frequencies lower than 200 Hz is measured separately by comparison of phases of chopping frequency components from photomultiplier tube and reference signal detector.

APPENDIX C

SYSTEM COMPONENT SPECIFICATION

Manufacturers' specification sheets are reproduced below for the following system components.

1. Ampex FR-1300 instrumentation tape recorder.
2. RCA - 6199 photomultiplier tube.
3. Venus Scientific photomultiplier high voltage supply.
4. United Detector Technology PIN-10 photodiode and preamplifier.
5. Trygon HR40-3B D.C. power supply.
6. Electro-Craft E-650 motor speed control system.

15 MAR '67 A
DO55S

AMPEX FR-1300
INSTRUMENTATION RECORDER

PERFORMANCE SPECIFICATIONS

General Description

The Ampex FR 1300 is a compact, lightweight portable recorder, available in 7 or 14 channel versions. It features an integral capstan servo system that assures speed accuracy under variable power conditions and provides electrical switching over a range of six speeds. For applications requiring precisely accurate speeds or where it is desired to record and reproduce on different recorders under unpredictable voltage conditions, a control track generator/demodulator module can easily be added to the integral capstan servo system to provide a complete record/reproduce tape speed servo control system (Speedlock). Transport control circuitry is completely interlocked to prevent tape damage if the recorder is operated carelessly or accidentally. Interchangeability of electronics is possible with nine other Ampex recorders using ES 100 electronics. Signal compatibility with earlier recorders having 100 Kc direct or 10 Kc FM capability is also provided. A rack mounted version is available.

Tape Transport

Tape Speeds: 60, 30, 15, 7½, 3¾, 1⅞ ips standard. All six transport speeds are selected by a single front panel control. All speeds are synchronously controlled by a phase locked servo system on capstan drive motor. Other fixed or variable speeds on special order.

Capstan Speed Accuracy: ±0.05% maximum, long term, when using the internal crystal reference. Frequency standard is accurate to ±0.01%, long term.

Tape Speed Deviation: ±0.25%

Reels: The FR 1300 tape transport accommodates 10½-inch reels Ampex Precision or NAB.

Tape Specifications. Available in versions for ½ or 1-inch tape of 1 mil or 1½ mil Polyester or 1½ mil Acetate. Stated performance guaranteed only when using recommended Ampex Instrumentation Tape.

Controls: Illuminated pushbuttons for Record, Drive, Stop, Forward and Rewind. All functions may be remotely controlled. Control circuitry is completely interlocked so that recorder can be switched from any mode to any other mode without damaging the tape.

Fast Wind Time: For 10½ inch reel, with 3600 feet of tape, approximately 3.0 minutes at 60 cycles per second (3.5 min. at 50 cps).

Start Time: Time required from start command to meet flutter specifications is as follows:

Speed (ips)	Time
60	8 seconds
30	6 seconds
15 and lower speeds	4 seconds

Stop Time: Maximum of 1.5 seconds at 60 ips tape speed, shorter stop times with lower tape speeds.

Flutter: Maximum cumulative flutter (% peak to-peak)

Tape Speed (ips)	Bandpass (cps)	Flutter (%)	Bandpass (cps)	Flutter (%)
60	0.2 to 10,000	0.6	0.2 to 312	0.20
30	0.2 to 5,000	0.6	0.2 to 312	0.25
15	0.2 to 2,500	0.6	0.2 to 312	0.4
7½	0.2 to 1,250	0.75	0.2 to 312	0.6
3¾	0.2 to 625	1.2	0.2 to 312	1.2
1⅞	0.2 to 312	1.5	0.2 to 312	1.5

Heads

Gap Scatter: Trailing edges for record heads (or gap centers for reproduce heads) within a band 100 microinches wide (0.0001 inch).

Gap Azimuth: All stacks within ±1 minute of arc perpendicular to head base plate.

Track Dimensions: Track width is 0.050 inch, tape track spacing 0.070 center (IRIG Standard). Other heads on special order.

Number of Tracks: 7 on ½ inch, 14 on 1 inch (IRIG Standard). Other heads on special order.

Interstack Spacing: 1.5 ±0.0005 inch, gap to gap.

Direct Record/Reproduce System

Frequency Response:

Tape Speed (ips)	Bandwidth	S/N* (db) Bandpass Filtered**	S/N* (db) Unfiltered
60	300 cps to 300 Kc ±3 db	35	31
30	150 cps to 150 Kc ±3 db	34	30
15	100 cps to 75 Kc ±3 db	32	27
7½	50 cps to 38 Kc ±3 db	30	22
3¾	50 cps to 19 Kc ±3 db	29	22
1⅞	50 cps to 10 Kc ±3 db	28	22

*For an all Direct system only. In a mixed Direct/FM system Direct S/N and crosstalk may be affected.
**Measured at output of a bandpass filter having 18 db/octave attenuation beyond limits stated.

RMS Signal-to-Noise Ratio: See table.

Harmonic Distortion: Less than 1.2% total of a 1 Kc signal recorded at 60 ips.

Input Level: 1.0 volt rms nominal (0 dbv) to produce normal recording level, operable from 0.2 to 10 volts rms by adjustment of input potentiometer.

Input Impedance: Nominal 50 K ohms resistive, in parallel with 150 pf, unbalanced to ground.

Output Level: 1.0 volt rms nominal (0 dbv), across a 600 ohms or greater impedance.

Output Impedance: Less than 50 ohms, unbalanced to ground.

FM Record/Reproduce System

Frequency Response:

Tape Speed	Frequency Response (within 1.0 db)	S/N Ratio RMS	Total Harmonic Distortion
60 ips	0 to 70,000 cps	46 db	1.2%
30 ips	0 to 36,000 cps	46 db	1.2
15 ips	0 to 14,000 cps	45 db	1.2
7½ ips	0 to 7,500 cps	45 db	1.2
3¾ ips	0 to 3,750 cps	42 db	1.5
1⅞ ips	0 to 625 cps	40 db	1.8

RMS Signal-to-Noise Ratio (at center carrier): See table.

Harmonic Distortion: See table.

DC Drift: Less than ±0.5% of full deviation over a four hour period after warmup (15 minutes). Less than 2% in 8 hours with temperature variations between +40° and 125°F.

continued

FM Record/Reproduce System (con't)

Record/Reproduce Voltage Linearity: ±0.75% of full band, of a zero based straight line

Input Level: *Input of 1 volt rms (0 dbv) to produce ±40% deviation,* operable from 0.5 to 25 volts rms by adjustment of input potentiometer

Input Impedance: Nominal 20,000 ohms resistive, in parallel with 150 pF, unbalanced to ground

Output Level: 1.0 volt rms (nominal) into 10 K ohms or greater load impedance

Output Impedance: 600 ohms, unbalanced to ground

PDM Record/Reproduce System (IRIG Compatible)

System Pulse Characteristics:

Tape Speed (ips)	Pulse Duration in Microseconds Min	Max.	Pulse Accuracy in Microseconds Over Specified Pulse Widths
60	20	10,000	±2.0 (30 to 900 μsec duration)
30	30	10,000	±2.0 (45 to 900 μsec duration)
15	60	10,000	±3.0 (60 to 2,000 μsec duration)
7½	120	10,000	±10.0 (120 to 3,000 μsec duration)

Input Level: 1 volt peak to-peak rectangular wave 20 microseconds to 10,000 microseconds pulse duration, operable from 0.75 to 20 volts peak to-peak.

Input Impedance: 20,000 ohms nominal paralleled by 150 pF maximum, unbalanced to ground.

Output Level: 20 to 24 volts peak to-peak across 1000 ohms and 0.001 mfd

Output Impedance: Less than 100 ohms, unbalanced to ground.

Output Rise and Fall Time: 2 microseconds maximum (from 10% to 90% amplitude level)

Servo Tape Speed Control System (Speedlock)

Frequency Standard Accuracy: ±0.01%, long term

Speed Correction Range: ±2% of nominal.

Servo Tape Speed Control System (con't)

Time Displacement Error

Tape Speed	Error
60 ips	100 microseconds
30 ips	150 microseconds
15 ips	200 microseconds

Synchronization Time: After 10 minute warmup

Tape Speed	Time
60 ips	8 seconds
30 ips	6 seconds
15 ips	4 seconds

Power Requirements

Voltage: 105 to 125 volts, single phase 48 to 62 cps AC (with Frequency Standard)

Power Consumption: *Less than 325 watts steady state for a 14 track* record/reproduce system Starting surges up to 400 watts may be encountered.

Environment

Temperature: Operating 5°C to 52°C (40°F to 125°F)
Storage/non operating, −30°C to 66°C (−20° to 150°F)

Altitude: Operating 15,000 feet (4600 m)
Non operating 50,000 feet (15,000 m)

Relative Humidity: 5 to 95%, non condensing, both operating and non operating

Vibration: Normal handling and transportation only

Physical Characteristics

Size: Portable case 24 inches (61 cm) high, by 18 inches (46 cm) wide, by 12½ inches (31 cm) deep, for complete 14 track *record/reproduce* system and capstan servo

Vertical Rack Space Required: Rack mounted version Transport 24½ inches (62.2 cm), electronics tray 5¼ inches Each electronics tray accommodates up to 14 record or reproduce modules, plus 3 *auxiliary modules.*

Weight: Portable version Approximately 110 lbs (50 kg) for 7 track system

METRIC CONVERSION TABLES

Applicable to all Ampex recorders—specific items may not apply to the unit described in this sheet

TAPE SPEEDS

ips	1⅞	3¾	7½	15	30	60	120
cm/sec	4 76	9 52	19 05	38 1	76 2	152 4	304 8

TAPE DIMENSIONS

Reels: inches	14	10½	7	5¾	5	
cm	35 56	26 67	17 78	14 62	12 70	
Widths: inches	¼	½	¾	1	2	
cm	0 635	1 27	1 905	2 54	5 08	
Base Thicknesses: inches		1 mil		1 5 mil		
mm		0 0254		0 0381		

TAPE DIMENSIONS (Continued)

Length: Feet	600	1200	1800	2500	3600	5000	7200	9600	
meters	185	366	549	762	1097	1524	2195	2926	

HEAD DIMENSIONS

Gap Scatter		Interstack Spacing*		Track Width & Spacing*	
microinches	100	inches	1 5 +0 0005	inches	0 050 0 070
mm	0 00254	cm	3 81 ±0 00127	mm	1 27 1 778
				*(IRIG)	

STANDARD PANELS FOR 19-INCH (48.26 cm) RACK

In.	1¾	3½	5¼	7	8¾	12¼	14	15¼	17½	19¼	21	35	
cm	4 45	8 89	13 34	17 78	22 23	31 12	35 56	40 01	44 45	48 9	53 34	88 9	

Ampex Corporation reserves the right to change specifications without notice or obligation This specification sheet supersedes all previous specifications, stated or implied

AMPEX CORPORATION
401 Broadway • Redwood City • California • U.S.A. • 94063
Australia, Canada, England, France, Germany, Hong Kong, Mexico, Switzerland

©1965 AMPEX CORPORATION

LITHO IN U.S.A.—D055BA 3-65

RCA-6199

PHOTOMULTIPLIER TUBE

10-Stage Head-On Type
S-11 Spectral Response

RCA-6199 is a 10-stage, head-on, 1½"-diameter type of photomultiplier tube intended for use in scintillation counters and for the detection and measurement of low-level radiation.

The spectral response of the 6199, at the 10-percent points, covers the approximate range from 3200 angstroms to 6100 angstroms as shown in *Fig. 1.* Maximum relative response occurs at about 4400 angstroms, and peak cathode quantum efficiency at about 4200 angstroms.

SPECTRAL RESPONSE CHARACTERISTICS

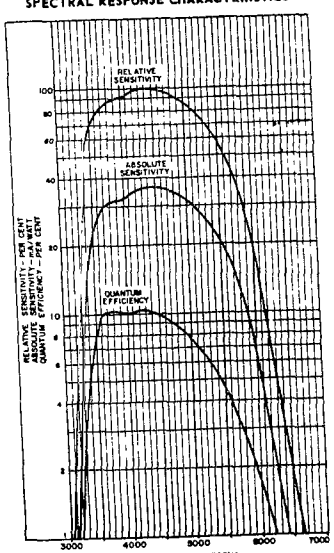

Fig. 1

FEATURES

- **Fast Time Resolution Characteristics –**
  Anode Pulse Rise Time:
  2.5 nanoseconds at 1250 volts
  Electron Transit Time:
  29 nanoseconds at 1250 volts
- **High *Current Amplification* –**
  1×10^6 at 1000 volts
- **Flat Faceplate for Ease in Scintillator Coupling**

DATA

General:

Spectral Response	S-11
Wavelength of Maximum Response	4400 ± 500 angstroms
Cathode, Semitransparent	Cesium-Antimony
Shape	Flat-Circular
Minimum area	1.2 in^2
Minimum diameter	1.24 in
Window	Lime Glass, Corning® 0080, or equivalent
Shape	Plano-Plano
Index of refraction at 5893 angstroms	1.51
Dynodes:	
Substrate	Nickel
Secondary-Emitting Surface	Cesium-Antimony
Structure	Circular-Cage
Direct Interelectrode Capacitances (Approx.):	
Anode to dynode No.10	4 pF
Anode to all other electrodes	7 pF
Maximum Overall Length	4.57 in
Seated Length	3.88 ± 0.19 in
Maximum Diameter	1.56 in
Bulb	T12
Base	Small-Shell Duodecal 12-Pin, (JEDEC No.B12-43), Non-hygroscopic
Socket	Eby[b] Part No.9058, or equivalent
Magnetic Shield	Millen[c] Part No.80602C, or equivalent
Operating Position	Any
Weight (Approx.)	2.2 oz

Maximum Ratings, *Absolute-Maximum Values:*[d]

DC Supply Voltage:	
Between anode and cathode	1250 max. volts
Between anode and dynode No.10	250 max. volts

Trademark(s) ® Registered
Marca(s) Registrada(s)

RADIO CORPORATION OF AMERICA
Electronic Components and Devices Harrison, N.J.

6199 6/66
Supersedes 6199 5/66
Printed in U.S.A.

Maximum Ratings (Cont'd)

Between consecutive dynodes . . .	200 max.	volts
Between dynode No.1 and cathode	300 max.	volts
Average Anode Current[e]	0.75 max.	mA
Ambient Temperature[f]	75 max.	°C

Characteristics Range Values for Equipment Design:

Under conditions with supply voltage (E) across voltage divider providing 1/6 of E between cathode and dynode No.1; 1/12 of E for each succeeding dynode stage; and 1/12 of E between dynode No.10 and anode.

With E = 1000 volts (Except as noted)

	Min.	*Typical*	*Max.*	
Sensitivity:				
Radiant[g] at 4400 angstroms . .	–	3.6×10^4	–	A/W
Cathode radiant[h] at 4400 angstroms . .	–	0.036	–	A/W
Luminous[i] .	10	45	300	A/lm
Cathode luminous:				
With tungsten light source[k]	3.0×10^{-5}	4.5×10^{-5}	–	A/lm
With blue light source[m]	2.8×10^{-8}	–	–	A
Cathode quantum efficiency at 4200 angstroms . .	–	10	–	%
Current Amplification . . .	–	1×10^6	–	
Equivalent Anode-Dark-Current Input[n]	–	2.3×10^{-10}p	2.5×10^{-9}p	lm
	–	2.8×10^{-13}q	3.1×10^{-12}q	W
Anode Dark Current[n,r] . .	–	4.5×10^{-9}	–	A
Dark Current to Any Electrode Except Anode (At 22° C)	–	–	7.5×10^{-7}	A
Equivalent Noise Input[t]	–	4×10^{-12}	1.7×10^{-11}	lm
	–	5×10^{-15}q	2.1×10^{-14}q	W
Anode-Pulse Rise Time[s] .	–	2.8×10^{-9}	–	sec
Electron Transit Time[t]	–	3.3×10^{-8}	–	sec

[a] Made by Corning Glass Works, Corning, New York.

[b] Made by Hugh H. Eby Company, 4701 Germantown Avenue, Philadelphia 44, Pa.

[c] Made by James Millen Manufacturing Company, 150 Exchange Street, Malden 48, Massachusetts.

[d] The *maximum ratings* in the tabulated data are established in accordance with the following definition of the *Absolute-Maximum Rating System* for rating electron devices. Absolute-Maximum ratings are limiting values of operating and environmental conditions applicable to any electron device of a specified type as defined by its published data, and should not be exceeded under the worst probable conditions.

The device manufacturer chooses these values to provide acceptable serviceability of the device, taking no responsibility for equipment variations, environment variations, and the effects of changes in operating conditions due to variations in device characteristics.

The equipment manufacturer should design so that initially and throughout life no Absolute-Maximum value for the intended service is exceeded with any device under the worst probable operating conditions with respect to supply-voltage variation, equipment component variation, equipment control adjustment, load variation, signal variation, environmental conditions, and variations in device characteristics.

[e] Averaged over any interval of 30 seconds maximum.

[f] Tube operation at room temperature or below is recommended.

[g] This value is calculated from the typical value for luminous sensitivity using a conversion factor of 804 lumens per watt.

[h] This value is calculated from the typical value for cathode luminous sensitivity using a conversion factor of 804 lumens per watt.

[i] Under the following conditions: The light source is a tungsten-filament lamp having a lime-glass envelope. It is operated at a color temperature of 2870° K and a light input of 10 microlumens is used.

[k] Under the following conditions: The light source is a tungsten-filament lamp having a lime-glass envelope. It is operated at a color temperature of 2870° K. The value of light flux is 0.01 lumen and 167 volts are applied between cathode and all other electrodes connected as anode.

[m] Under the following conditions: Light incident on the cathode is transmitted through a blue filter (Corning C.S. No. 5-58, Glass Code No.5113 polished to 1/2 stock thickness-Manufactured by the Corning Glass Works, Corning, New York) from a tungsten-filament lamp operated at a color temperature of 2870° K. The value of light flux incident on the filter is 0.01 lumen and 167 volts are applied between cathode and all other electrodes connected as anode.

[n] Measured at a tube temperature of 22° C. Dark current may be reduced by use of a refrigerant.

[p] Measured with supply voltage (E) adjusted to give a luminous sensitivity of 20 amperes per lumen. Dark current is measured with no incident light on tube.

VSI **VENUS SCIENTIFIC INC.**

PHOTOMULTIPLIER POWER SUPPLY

MODEL K 15 *Reliable • Efficient • Compact • Versatile*

Photo 2 x Actual Size

- 1500 Volts @ 1ma
- $E_{out} \cong 100 \times E_{in}$
- **Reverse Polarity Protected**
- Efficiency > 50%
- Ripple < 0.1% Peak-Peak
- **Short Circuit Protected**
- M.T.B.F. 105,000 Hrs.
- Output isolated from Input
- **All Silicon Components**

The K15 is a high voltage power supply whose versatility makes it a very useful component in a number of applications. The unit is fully encapsulated and shielded in a nickel-plated steel can. The two output high voltage leads are floating and are fully isolated from the two input leads. This permits operation from voltage sources having either plus or minus polarity while still allowing the user to employ the unit as a plus or minus high voltage power supply. In addition, the case is isolated from both input and output and can be grounded by the user at a remote point. The high voltage filter capacitor inside the unit is .006 uf at 3 KV. This keeps the ripple at full load down to 0.1%. Where even less ripple is desired, the addition of .01 uf across the output will reduce this figure to approximately 0.03%.

The K15 is protected against improper polarity voltages applied to its input by a series diode. The presence of this protective diode accounts for the most part for the temperature coefficient of output voltage of +0.02%/°C.

The K15 is 100% tested to guarantee reliable trouble-free operation to the user. The electrical operating characteristics for a typical unit are shown on the graph for input voltages of 3 volts to 15VDC and loads of 10 megs and 1.25 megs. A plot of input current as a function of input and loads is also included. From this plot it can be seen that the operating efficiency of the K15 is better than 50% for a load of 1 ma.

Applications: Photomultipliers . . . Flying spot scanners . . . Image dissectors . . . Ionization chambers . . . Scan converters . . . Geiger tubes . . . Cathode ray tube bias supply . . . Scintillation tubes.

Model K15U: For those users requiring fast response to input voltage changes, the K15 can be supplied without internal capacitors. This will enable the user to arrive at the best compromise between response time and output ripple.

VENUS SCIENTIFIC INC., 25 Bloomingdale Road, Hicksville, L. I., N. Y. 11801 Telephone 516—433-3360

MODEL K-15

(Electrical Characteristics)

Temp = +25°C
Ripple = 0.1%

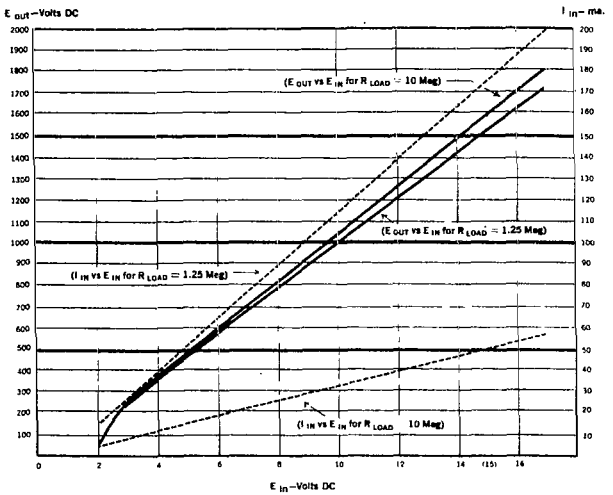

PHYSICAL SPECIFICATIONS

Dimensions	1" dia x 2¼" length
Volume	1.8 cu. in
Weight	3.5 ounces
Shock	40 g's per MIL-STD-810, Method 516, Procedure IV
Vibration	20 g's per MIL-STD-810, Method 514, Curve E, Figure 514-3
Acceleration	MIL-STD-810, Method 513
Thermal Shock	—54°C to + 71°C per MIL-STD-810, Method 504, Class 2
Finish, Case	Bright Nickel Plate
Can	cold rolled steel

ELECTRICAL SPECIFICATIONS

E output proportional to E input (see curve above)

Floating Output	2500V insulation strength with respect to input ground
Temperature	—55°C to + 71°C (operating)

Temperature coefficient is less than .02%/°C

Efficiency > 50% @ full load

M T B F 105,000 Hrs @ 71°C. (Mil-hdbk 217-A)

Electrical connections as shown below

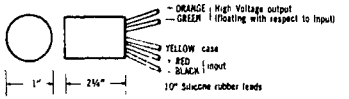

Brochure No K15-A-111067

VENUS SCIENTIFIC INC., 25 Bloomingdale Road, Hicksville, L. I., N. Y. 11801 Telephone 516—433-3360

FET Model 100 PREAMPLIFIER

- Ultra Low Noise
- Ultra Compact
- Battery Powered
- Preamplifier

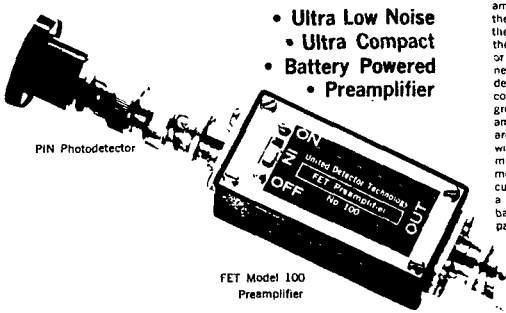

The UDT Model 100 is an ultra compact, ultra low noise FET preamplifier. The amplifier is especially designed for use with high impedance radiation detectors such as silicon photodiodes. An internal battery powers the amplifier as well as providing a bias voltage for the photodiode. It is only necessary to connect the photodiode to the input BNC connector of the Model 100 amplifier, and an oscilloscope or AC vtvm to the amplifier output BNC connector to form an extremely sensitive photodetection system. The internal batteries and completely shielded case enclosure eliminate ground loop hum pick up in the Model 100 amplifier. Ultra low noise discrete components are used throughout the amplifier, yielding a wideband input noise voltage of less than 15 microvolts rms. The input impedance is 1 megohm, giving a wideband noise equivalent current input of less than 15 picoamperes, and a N E P for silicon photodiodes and narrow bandwidths of less than 10^{-12} watts. The passband is within 3 db from 3 cps to 75 kc, the gain bandwidth product extends beyond 1 mc, and the risetime is less than 5 microseconds.

...ATURES OF THE FET Model 100 .....

...power requirements for the amplifier.

...PROTECTION — The internal battery provides a 6-volt reverse bias voltage for a silicon ..., and a 2-megohm load resistor is located in the input.

...components are used throughout. The wide band wideband noise level ... than, in 10 cps rms. A minimum detectable light power of less than 10^{-12} watts ... band and a narrow bandwidth output display.

PASSBAND — 1 cps to 100 kc.

UNITED DETECTOR TECHNOLOGY

P.O. Box 2251
Santa Monica, California 90405, U.S.A.
Phone: (213) 393-3785

SPECIFICATIONS – FET Model 100 PREAMPLIFIER

Voltage Gain	100, 40 db
Frequency Response	3 db, 1 cps – 75 kc
Input Impedance	1 megohm
Output Impedance	10 kilohm
Noise	<15 μv rms
Output Maximum	1 volt, rms
Power	Internal 6 v battery
Battery Life	Approximately 150 hours
Temperature Range	0 – 50°C

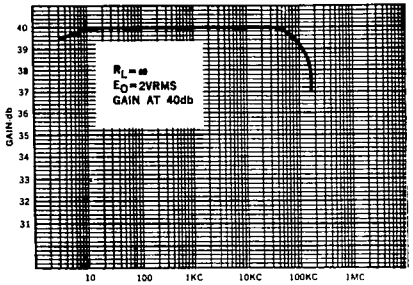

FREQUENCY RESPONSE – FET 100

CONNECTION TO PHOTODIODE

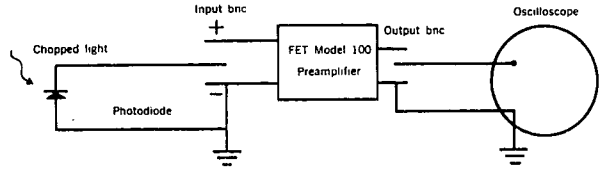

MECHANICAL DETAIL

CONN: 1st END — BNC Receptacle Jack, UG290A/U.

CONN: 2nd END — BNC Receptacle Jack, UG290A/U.

Anodized Finish Die Cast Aluminum

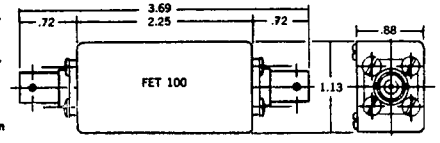

ORDERING INFORMATION

ORDER FROM: United Detector Technology, P.O. Box 2251, Santa Monica, California 90405 U.S.A.
PHONE (213) 457-2314
SHIPPED: Air Express, Prepaid within Continental U.S.A.
DELIVERY: 14 days.
TERMS Net 30 days

PiN-10

FAST, SENSITIVE, LARGE AREA PHOTODETECTOR FOR LIGHT DETECTION APPLICATIONS

PIN-10's exclusive combination of characteristics, not available in other photodetectors, makes it ideally suited for a wide variety of radiation detection applications. Among these are LASER systems, spectrometer systems, pattern recognition systems, light waveform and color detection systems

Only PiN-10 offers all these features, plus reasonable pricing, each $39. ppd. in quantity of ten or less.

SPECTRAL RESPONSE The PIN-10 covers three times as many angstrom units as a photomultiplier and has a short wave length response not obtained in ordinary silicon pn detectors. Spectral response is from ultra-violet to near infrared.

SPEED The PIN-10 is faster than any other solid state detector, as fast as a photomultiplier, and 100 times faster than ordinary silicon pn. Response time is measured in nano-seconds.

SIZE Large active area of 3 cm².

SENSITIVITY The PIN-10 offers response from ultraviolet to near infrared range, yet it has a detectivity as large as PbS. The dark current is less than a microampere, while the light current for a few foot-candles illumination is greater than a milliampere, allowing the use of PIN-10 in unchopped light applications.

Simple circuitry requirements... Convenient mounting in one inch lens holder... BNC connector termination on sealed package... Order from:

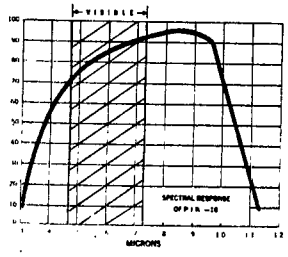

UNITED DETECTOR TECHNOLOGY

PiN-10

P.O. Box 2251
Santa Monica, Calif.

TRANSISTORIZED POWER SUPPLIES

MEDIUM POWER HALF RACK SERIES

CONSTANT VOLTAGE/CONSTANT CURRENT

OUTPUT: 0-20 VDC/0-40 VDC /0-80 VDC/0-160 VDC

REGULATION, LINE: 0.01% or 2 mv

LOAD: 0.01% or 5 mv

RIPPLE: Less than 0.5 mv RMS

INPUT: 105-125 VAC, 55-65 cps

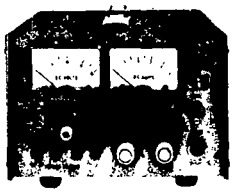

FEATURES

- ALL SILICON DESIGN
- TRYLINK PRECISION CURRENT REGULATION MODE
- MODE INDICATOR LIGHT
- AUTOMATIC SHORT CIRCUIT PROTECTION
- REMOTE VOLTAGE PROGRAMMING
- REMOTE SENSING
- SERIES OR PARALLEL OPERATION
- NO TURN ON/TURN OFF TRANSIENTS
- OVERVOLTAGE PROTECTION OPTION

ELECTRICAL SPECIFICATIONS

CONSTANT VOLTAGE MODE WITH ADJUSTABLE CURRENT LIMITING

INPUT: 105-125 VAC, 55-65 cps. (200-240 VAC, 50, or 400 cps available).
Output: Floating; isolated from ground, 300 VDC max.
REGULATION LINE: 0.01% or 2 mv,* for 105-125 VAC line change, at any output within specifications.
Regulation, Load: 0.01% or 3 mv,* no load to full load at any output within specifications.
Ripple: Less than 0.5 mv RMS.
Stability: 0.05% or 10 mv* for 8 hours after warm-up. Measured at constant line voltage, load and ambient temperature.
Temperature Coefficient: (0.02% + 400 μV)/°C.
High Stability Option (Zt): 0.01% or 2 mv* with a T.C. of (0.01% + 100μV)/°C.
Temperature Range: −20°C to + 80°C.
Recovery Time: Less than 50 microseconds to recover within 0.25% or 15 mv* of output voltage for 100% step change in rated load.
Short Circuit Protection: Automatic Adjustable Current Limiting (ACL) variable from 1% to 100% of rated current.
AC Power Input Protection: Fuse.
Remote Programming: All units remotely programmable over output voltage range. Scale factor approximately 100 ohms/volt.
Remote Sensing: Maintains rated regulation *directly* at the load. Maximum line drop 0.5 volts per leg.
Voltage Adjustment Range: Continuously adjustable concentric vernier controls.

CONSTANT CURRENT MODE WITH ADJUSTABLE VOLTAGE LIMITING

Current Range: 1% to rated current output.
Voltage Compliance: 0 to rated output voltage.
Regulation, Line: 0.5% I_{max} for 105-125 VAC line change at any output within specifications.
Regulation, Load: 0.5% I_{max} output current change for the maximum change in load resistance within the rated voltage compliance range.
Ripple: 0.25% or 5 ma.*
Stability: 0.5% I_{max} for 8 hours after warm-up. Measured at constant line voltage, load and ambient temperature.
Temperature Coefficient: 0.1% I_{max}/°C.
Remote Programming: Available on special order.

TRYLINK PRECISION CURRENT REGULATION MODE

Current Range: 1% to rated current output.
Voltage Compliance: 0 to rated output voltage.
Regulation Band: 0.1% I_{max} total — line regulation, load regulation, and 8 hour stability (after warm-up)—for any input or output within specifications.
Ripple: 0.02% or 1 ma.*
Temperature Coefficient: 0.1% I_{max}/°C.
*Whichever is greater

TABLE 1

Model	OUTPUT Volts	OUTPUT Amps	*Impedance (Zt)	DIMENSIONS W	H	D	Weight (lbs.)
[illegible]	0-20	0-5	0.004	7⅛	4⅜	14	25
[illegible]	0-20	0-10	0.002	7⅛	4⅜	14	27
[illegible]	0-40	0-3	0.008	7⅛	4⅜	14	25
[illegible]	0-40	0-5	0.004	7⅛	4⅜	14	26
[illegible]	0-40	0-7.5	0.004	7⅛	4⅜	14	26
[illegible]	0-80	0-2.5	0.008	7⅛	4⅜	14	25
[illegible]	0-80	0-5	0.004	7⅛	4⅜	14	26
[illegible]	0-160	0-2	0.008	7⅛	4⅜	14	26

*Nominal

GENERAL AND PHYSICAL SPECIFICATIONS

Operational Modes: Constant Voltage with adjustable current limiting; Constant Current with adjustable voltage limiting; Automatic Crossover; TRYLINK Precision Constant Current with adjustable voltage limiting.

Mode Indication: Front panel mode indicator light indicates when supply is operating in the constant current or current limiting mode.

Controls:
Voltage: Coarse and Fine; 0 to rated output; front panel.
Current: Coarse and Fine; 1% I_{max} to rated output; front panel.
Input Power: Front panel switch and indicator.

Metering:
Voltage: Front panel voltmeter.
Current: Front panel ammeter.

Terminals:
Front Panel: Pos. Output (+V) — Neg. Output (−V) — Pos. Sensing (+S) — Neg. Sensing (−S) — Ground (G).
Rear Panel: Pos. Output (+V) — Neg. Output (−V) — Pos. Sensing (+S) — Neg. Sensing (−S) — Ground (G) — Remote Voltage Programming (RVP) — Remote Current Programming (if included) (RIP) — TRYLINK connection (I, C)

Rack Mounting: RPA-1 (Single), RPA-2 (Dual) rack adapters, mounts two units side by side, 5¼" rack height, VPA-2 (Dual) rack adapter, mounts two units vertically.

BULLETIN No ES-60/65

MOTOMATIC®

Transistorized Motor Speed Control Systems

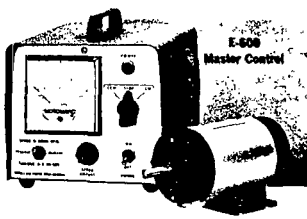

E-600 Master Control

SPECIFICATIONS

	E-600	E-650
SPEED RANGE:	1000:1. Typically 3 rpm to 3000 rpm. Down to 0.001 rpm with gearheads. (All systems reversible.)	
TORQUE RANGE: (Continuous)	6-3 lb.-in. (With gearhead up to 100 lb.-in.)	4-3 lb.-in.
MAXIMUM OUTPUT POWER: (Continuous)	55 watts at 1500 rpm	300 watts at 15
[illegible]	[illegible]	[illegible]

E-600 Motor Generator

ADDITIONAL FEATURES: Full torque and smooth cogging free shaft rotation even at lowest speeds. Temperature compensated generator for long term stability. Shielded ball bearings

TOMCO
Md - Va - D C
Long Point on Severn
Crownsville Maryland
Phone (301) 849 - 2401

Available as a Complete Packaged System or Unwired Component *System*

MOTOMATIC is a unique* dc servo motor and speed control system designed, engineered and manufactured by Electro Craft Corporation. MOTOMATIC is not an SCR type motor speed control MOTOMATIC is a complete closed loop system consisting of a fast response permanent magnet motor generator and transistorized velocity feedback amplifier MOTOMATIC *systems offer precise speed* control even in the presence of changing load conditions and line voltage

SPEED RANGE

MOTOMATIC systems have a nominal speed range of 1000:1, for example, 3 rpm to 3000 rpm for a standard E-600 system Compare this with 6:1 for "open-loop" control or 20:1 for better quality SCR controls *Typical* MOTOMATIC *speed, torque* and output power ranges are given for both E-600 and E-650 systems under SPECIFICATIONS. Standard gearmotor options allow an even greater selection of speed and load combinations. Electro-Craft motor-generators are quality engineered and manufactured to exacting specifications. Typical brush life is over 5000 hours at rated speed, as proven by more than 200,000 systems in the field Refer to Bulletin No EM-60/65 for motor-generator specifications.

CONTROLS

The E-600 M Master control includes speed control, zero to 3000 rpm electronic tachometer, torque monitor, adjustable torque limiting, reversing-brake switch and remote control capabilities Standard control E-600 S is basically the same as the E-600 M control but without tachometer, remote control and torque monitor The E-600 O open chassis version is similar to the E-600 S *except is assembled on an open chassis for* installation into customer's enclosure The speed control potentiometer, pilot light and switches are supplied loose for installation in user's control panel

Precision E-650 controls are similarly available as master, standard, open chassis and unwired systems Heavy duty power supply, high output transistors in the control and high efficiency *oriented ferrite magnets* in the motor, boost the E-650 system capabilities All E-600/650 series control amplifiers have "zero drift" differential input stage

Numerous specially designed MOTOMATIC systems have been manufactured to meet the needs of customers whose specifications call for non-standard motor and control configurations Determine your need and let Electro-Craft assume full system design, production, and quality control responsibility Please submit complete details of your application to permit our engineers to make a proposal

E-650 MG Motor Generator

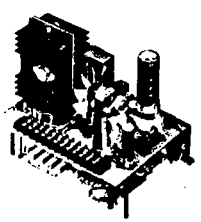

E-650 O Open Chassis Control

*Patents Pending

Litho In U S A

SOME MOTOMATIC APPLICATIONS

Office Copying Machines	Cameras	Photographic and Film Processing Equipment
Micro-Film Reader-Printers	Viscosimeters	Automatic Assembly Machines
Medical Equipment	Timing Devices	Machine Tool Programmers
Accurate Metering Pumps	Welding Feeds	Computer Equipment
Laboratory Instruments	Paper Chart Drives	over 400 different applications
Material Handling Equipment	Textile Machines	

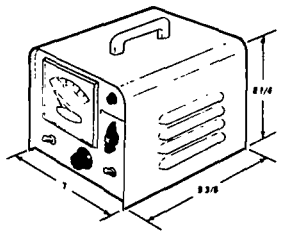

E-600 M Master Control
Weight: 8 lbs. 11 oz.

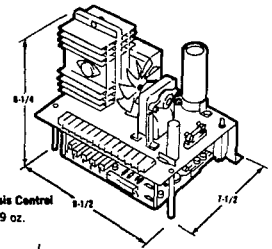

E-650 D Open Chassis Control
Weight: 6 lbs. 9 oz.

OUTLINE DIAGRAMS

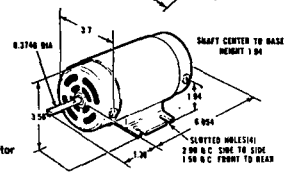

E-600/650 MG Motor Generator
Weight: 6 lbs

PERFORMANCE SPECIFICATIONS

Overall system regulation is represented by the speed-torque curves shown. MOTOMATIC E-600/650 systems are designed for operation within an ambient temperature range not exceeding 0-35°C and up to 50°C with 20% derating. When subjected to load torque changes less than 50% of full load torque a system speed regulation for the E-600 of better than 1% may be expected over a large part of the operating range of the system. E-650 systems include a special low drift amplifier and low regulation motors. These systems maintain an overall speed accuracy of better than 0.5% over the greater part of the system dynamic range

E-600 SYSTEM PERFORMANCE

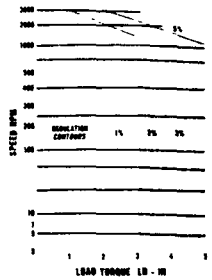

E-650 SYSTEM PERFORMANCE

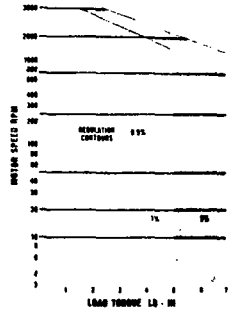

ELECTRO-CRAFT CORPORATION
1600 Second Street South, Hopkins, Minn 55343 - Tel (612)935-8226

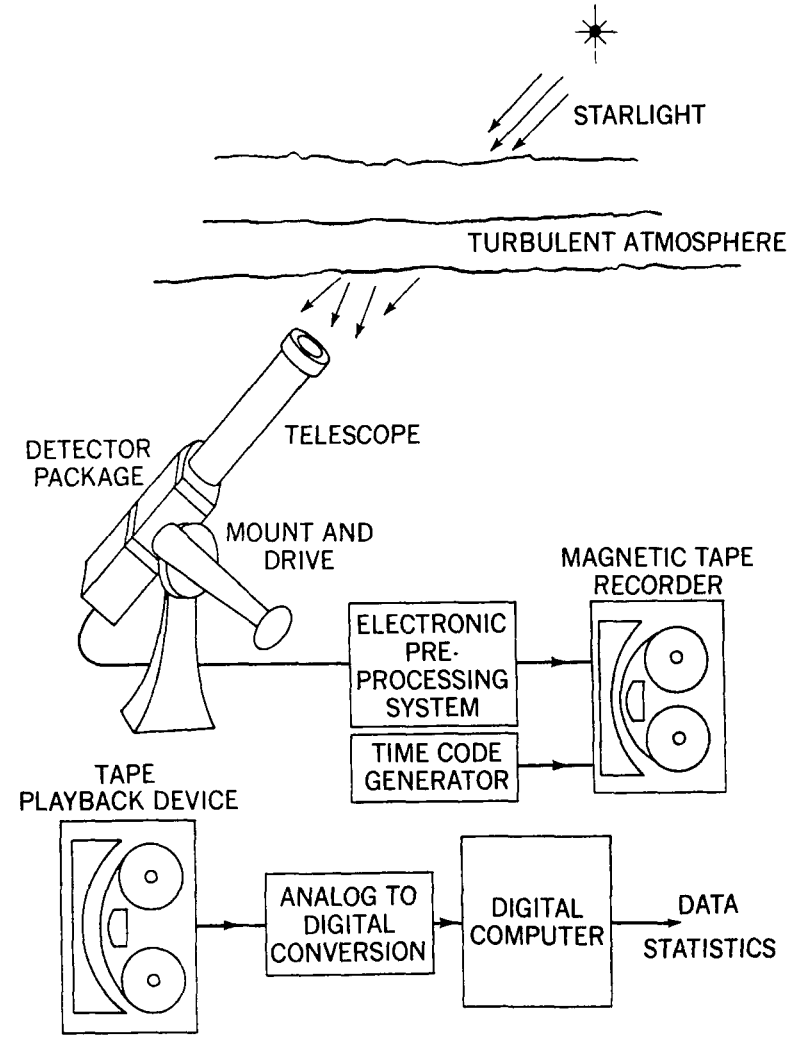

Figure 1. Stellar Image Monitor Experiment Concept

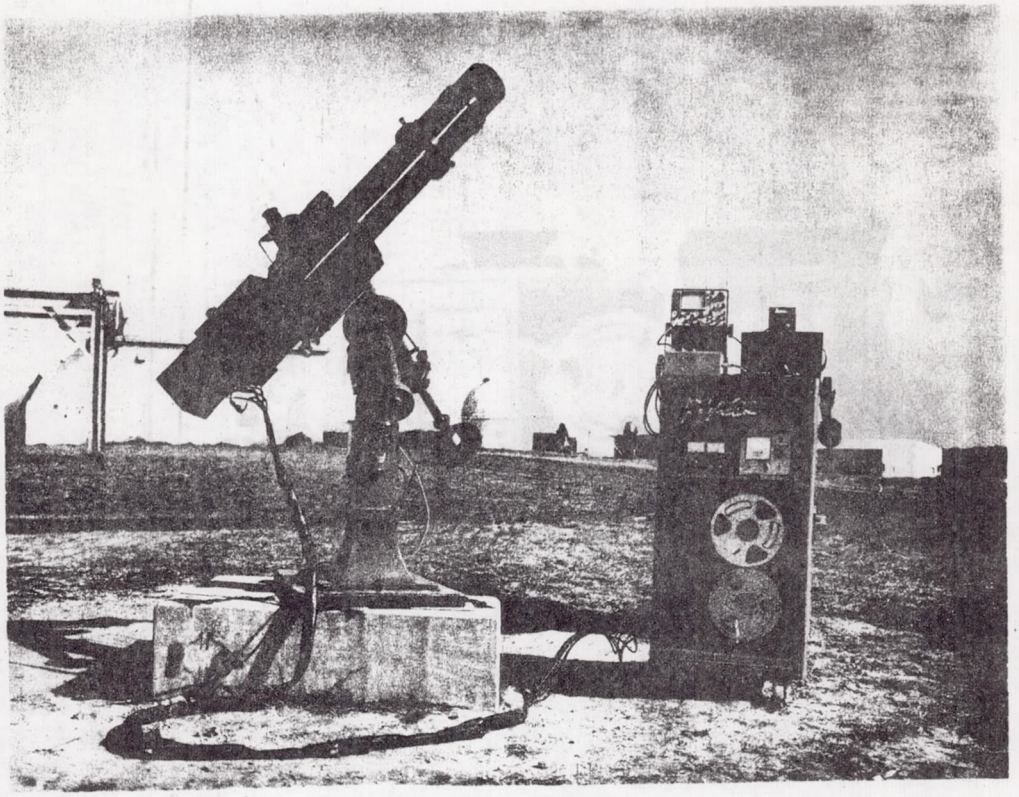

Figure 2. Stellar Image Monitor Field Equipment

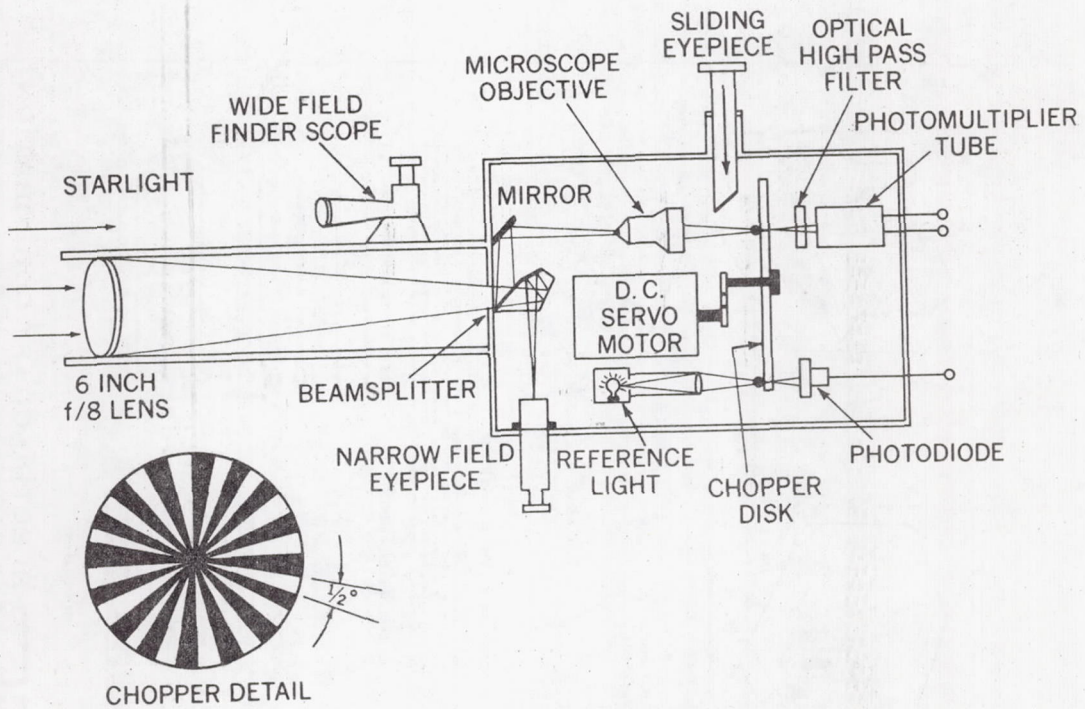

Figure 3. Optical System and Detector Package

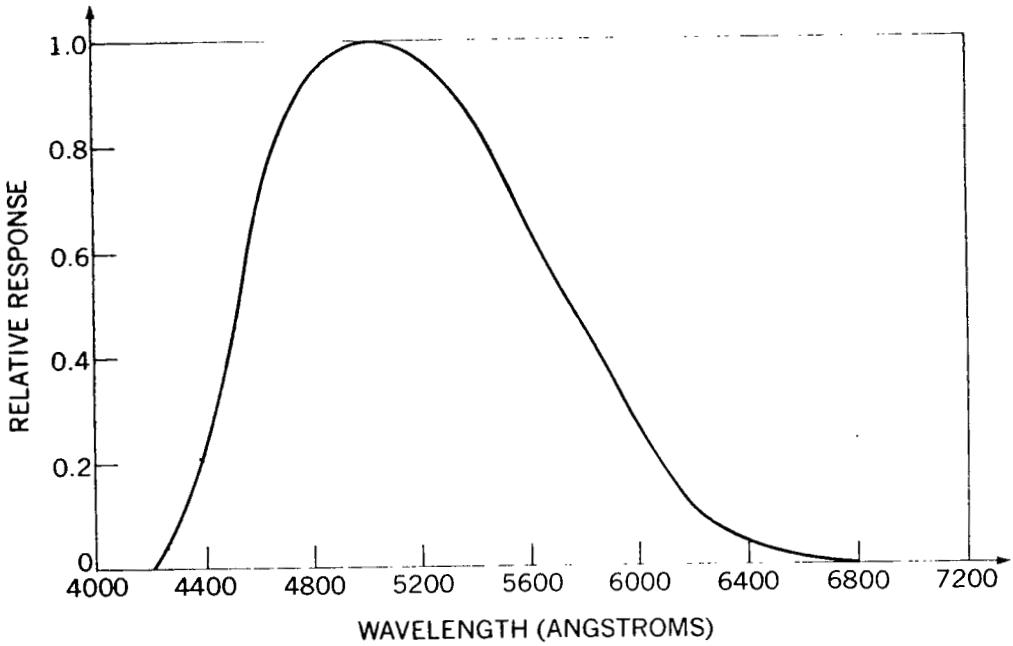

Figure 4. Combined Relative Spectral Response

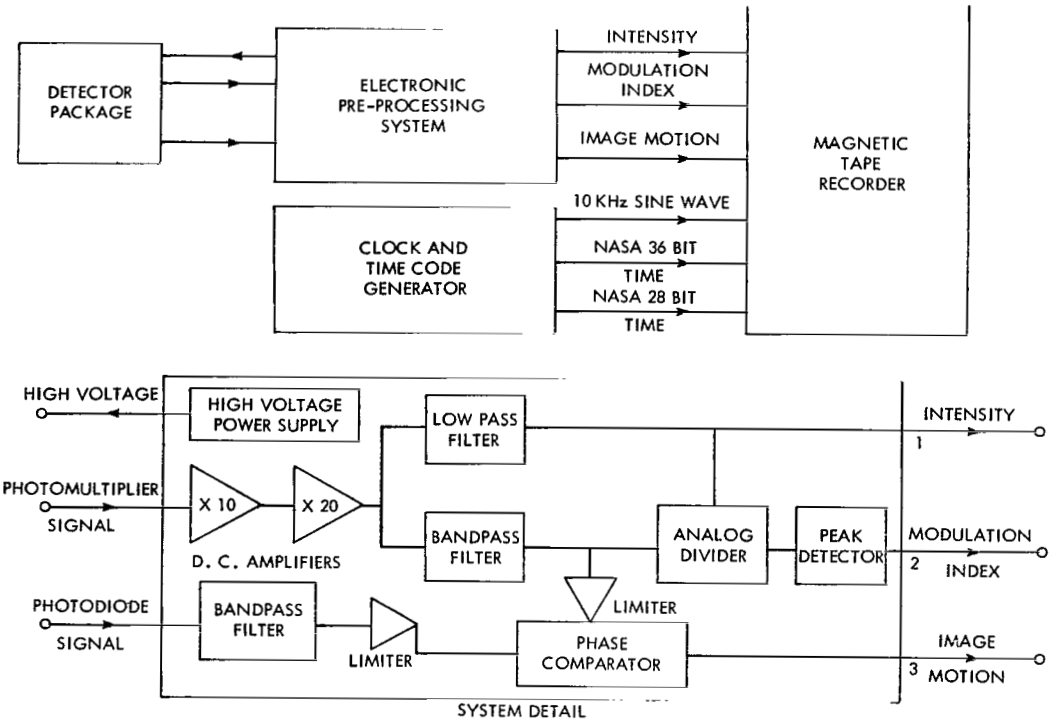

Figure 5. Electronic Pre-processing System

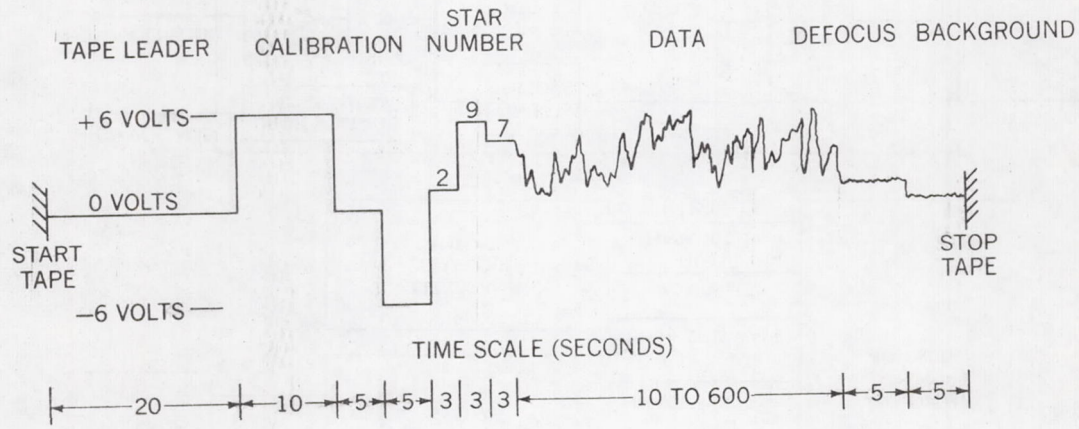

Figure 6. Data Run Format

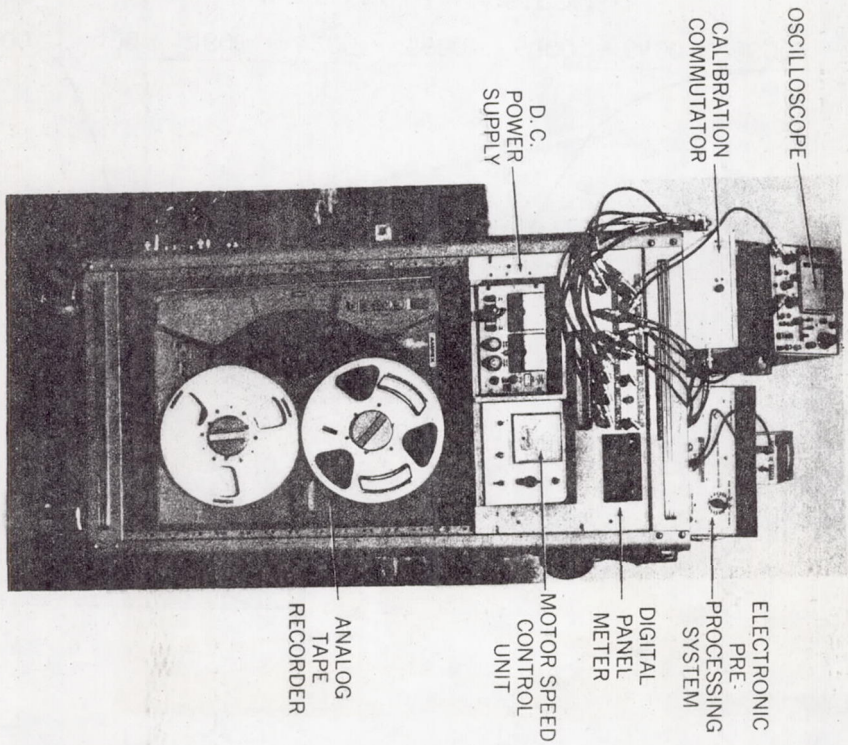

Figure 7. Detail of Electronic Data Collection Equipment

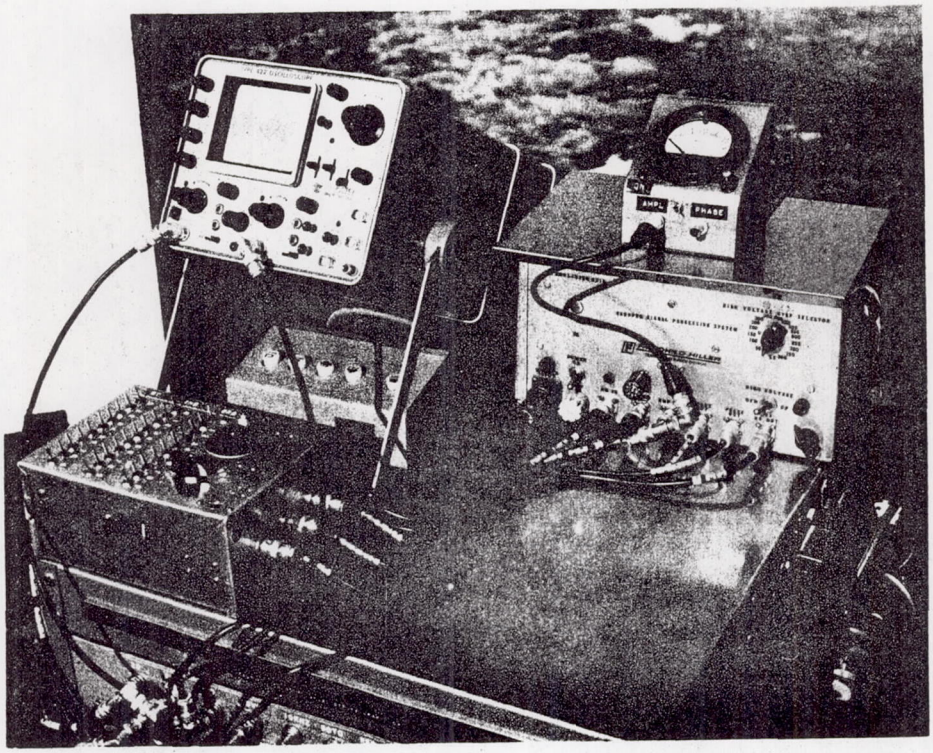

Figure 8. Detail of Electronic Data Collection Equipment

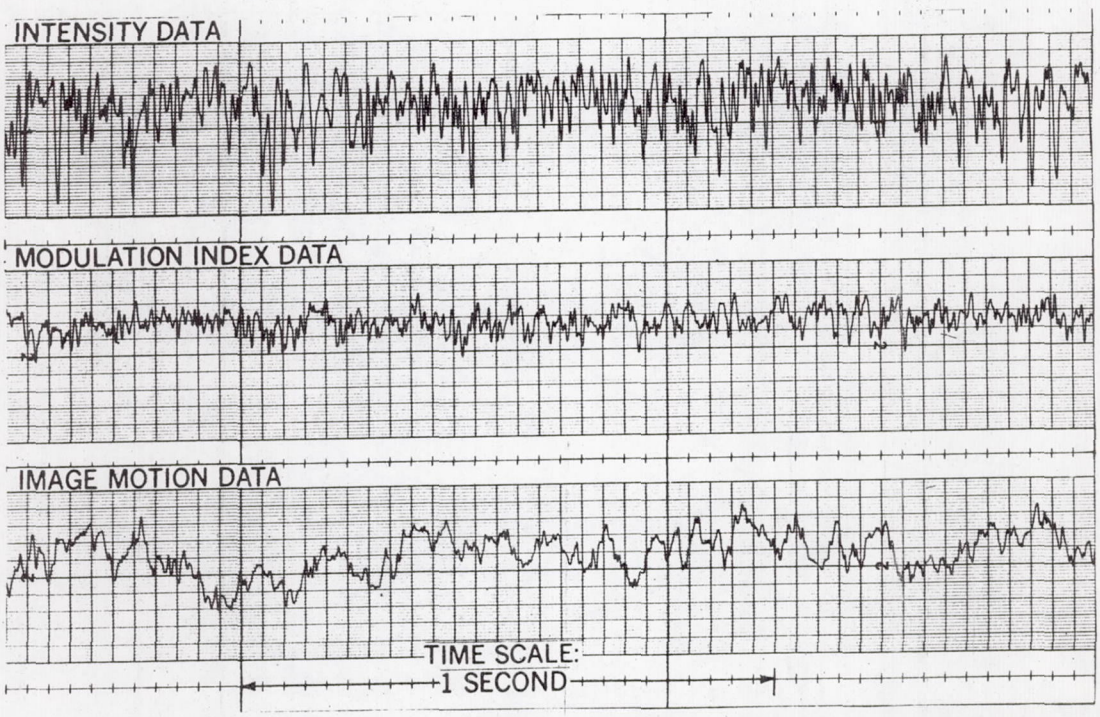

Figure 9. Typical Data Signals

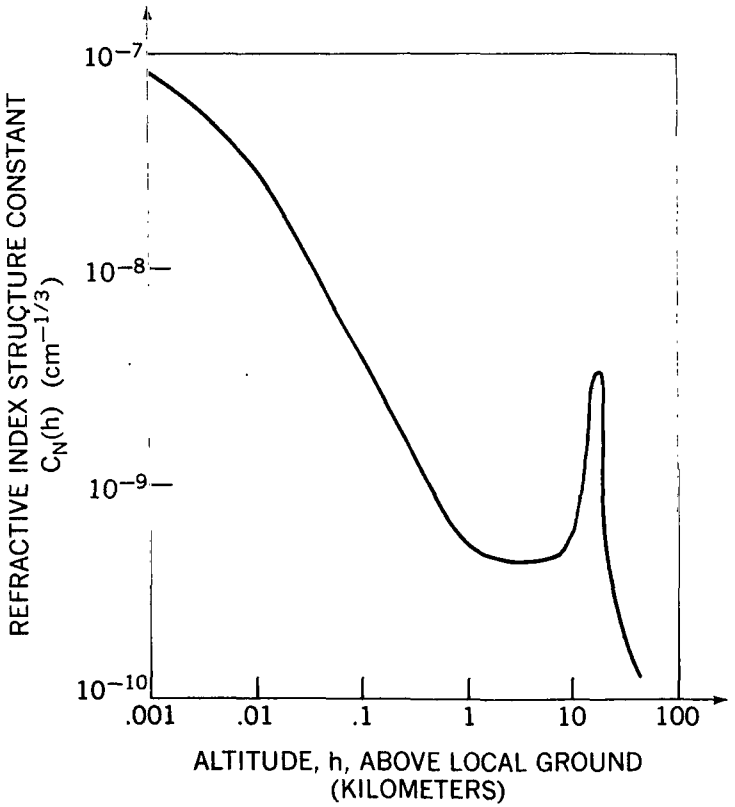

Figure 10. Average Nighttime Turbulent Profile

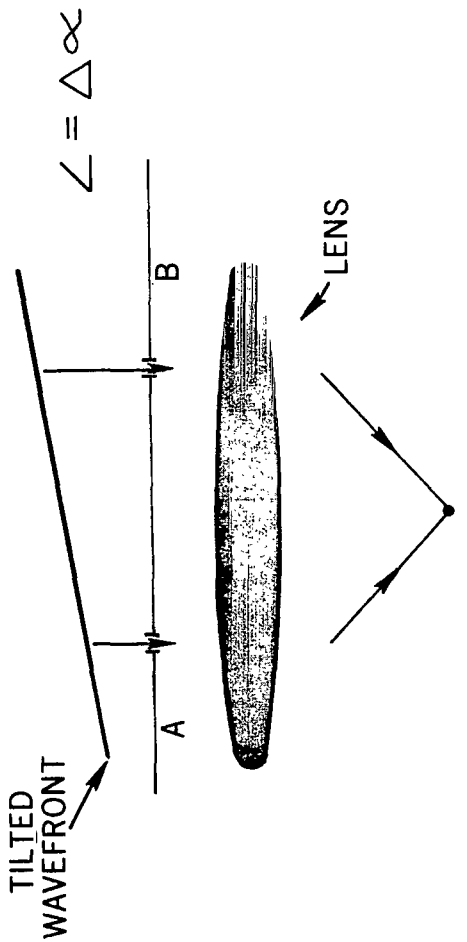

Figure 11. Wavefront Tilt in the Interferometer Case

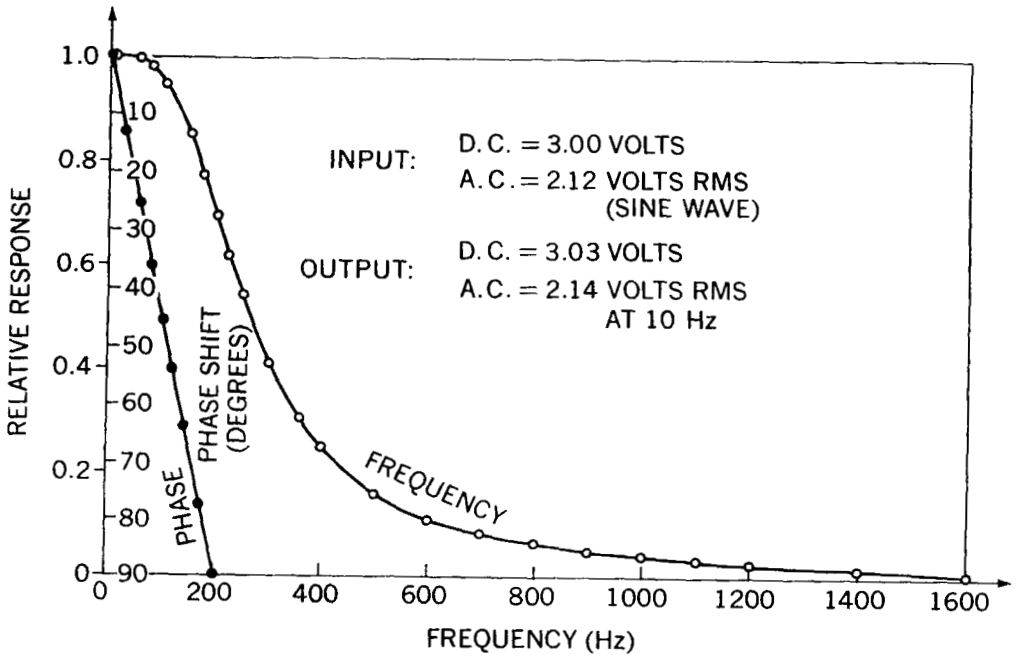

Figure 12. Lowpass Filter Frequency Response

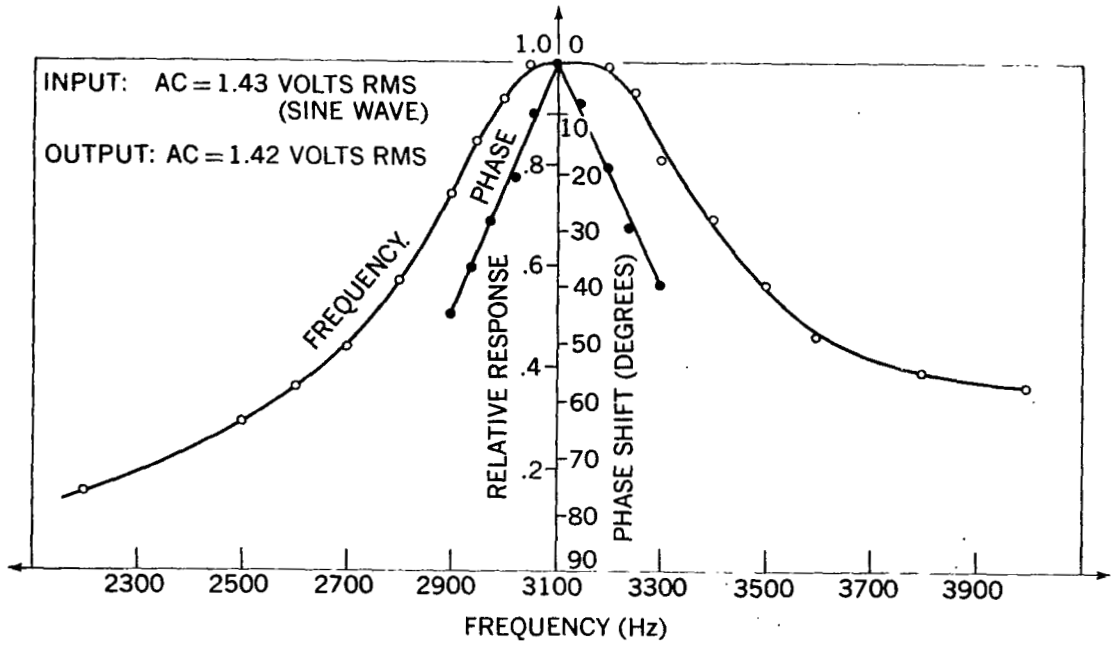

Figure 13. Bandpass Filter Frequency Response

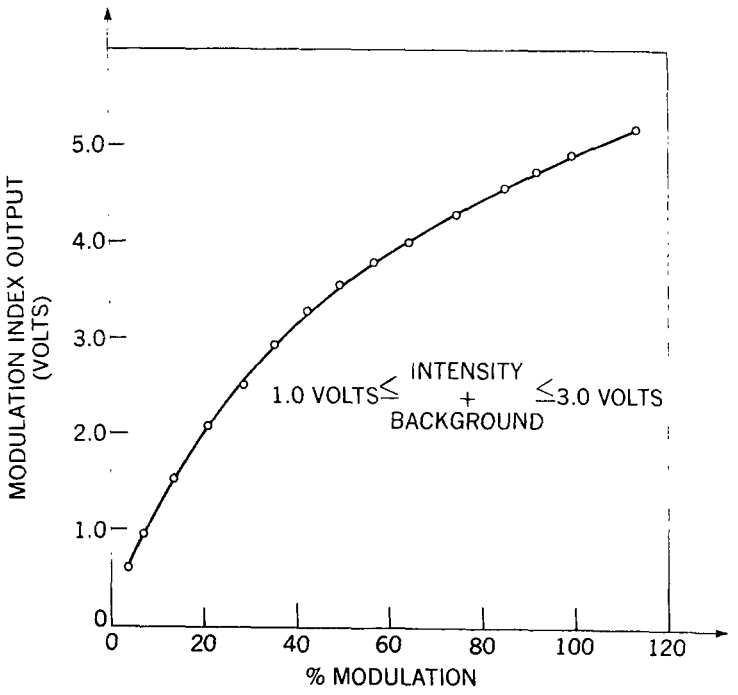

Figure 14. Laboratory Calibration of Modulation Index

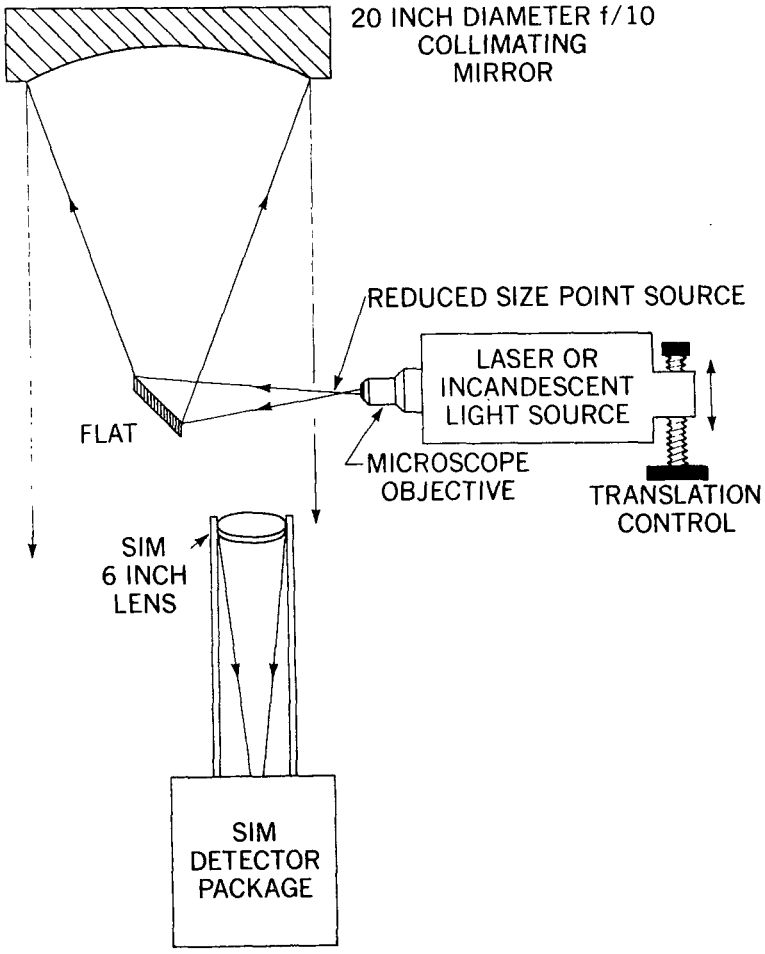

Figure 15. Laboratory Optical Test Setup

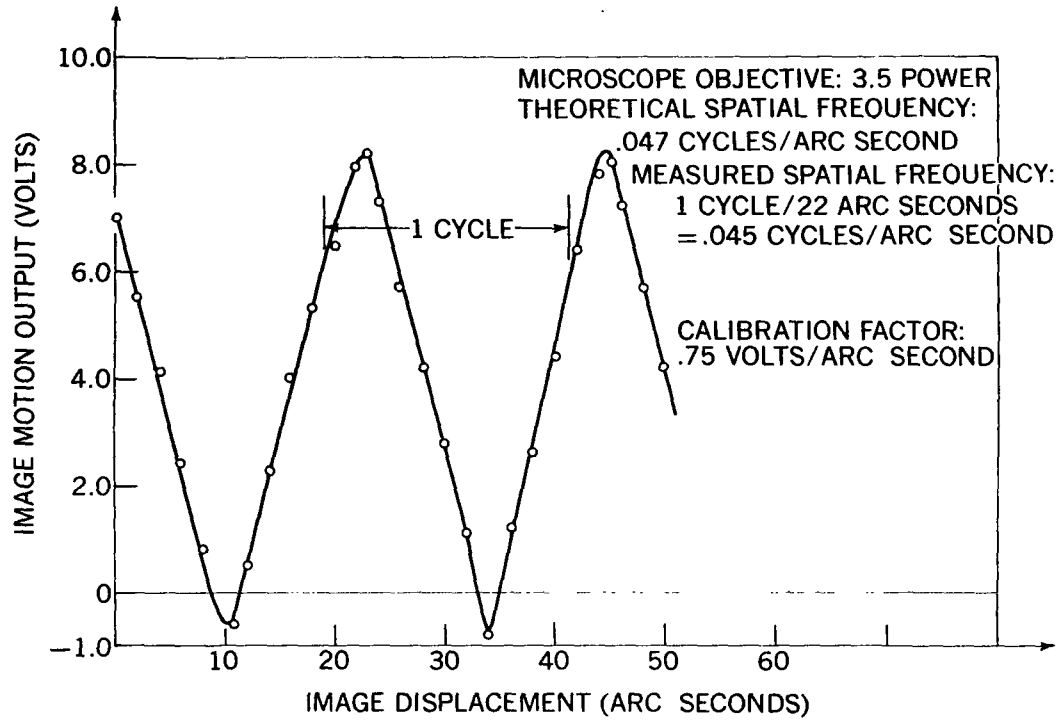

100

Figure 16. Laboratory Calibration of Image Motion

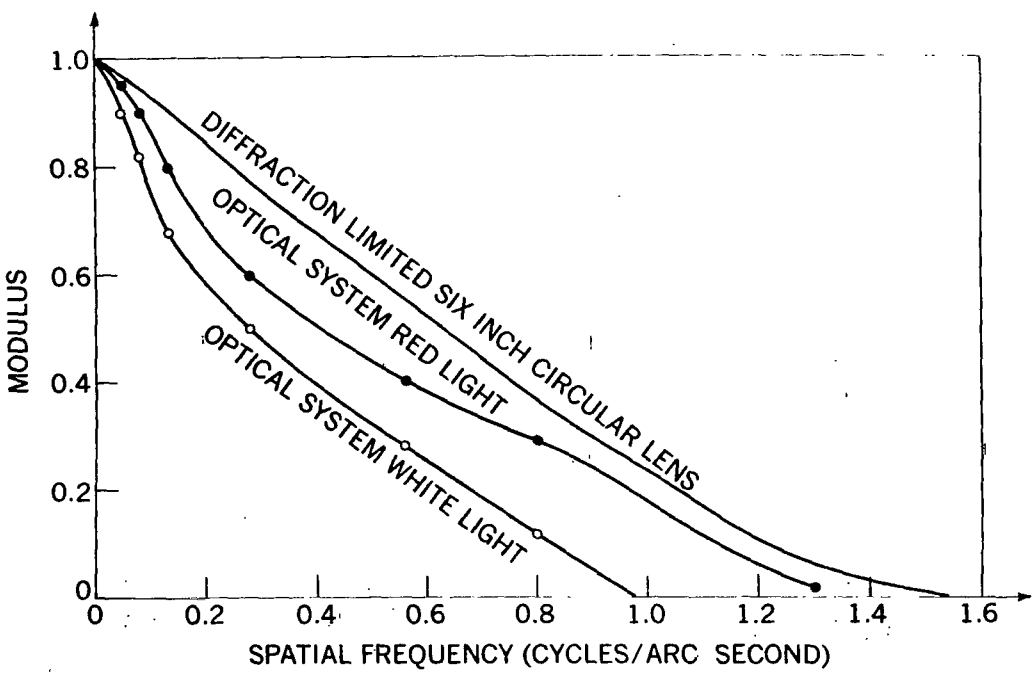

101

Figure 17. Laboratory Optical Transfer Functions

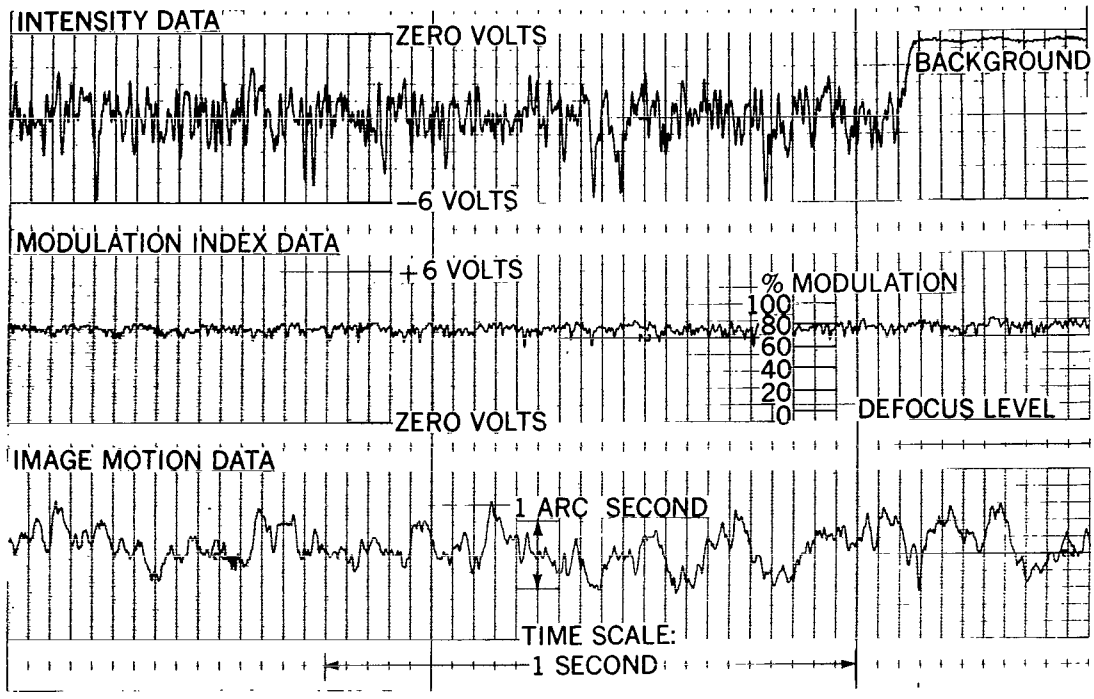

102

Figure 18. Chart Recordings of Data Run

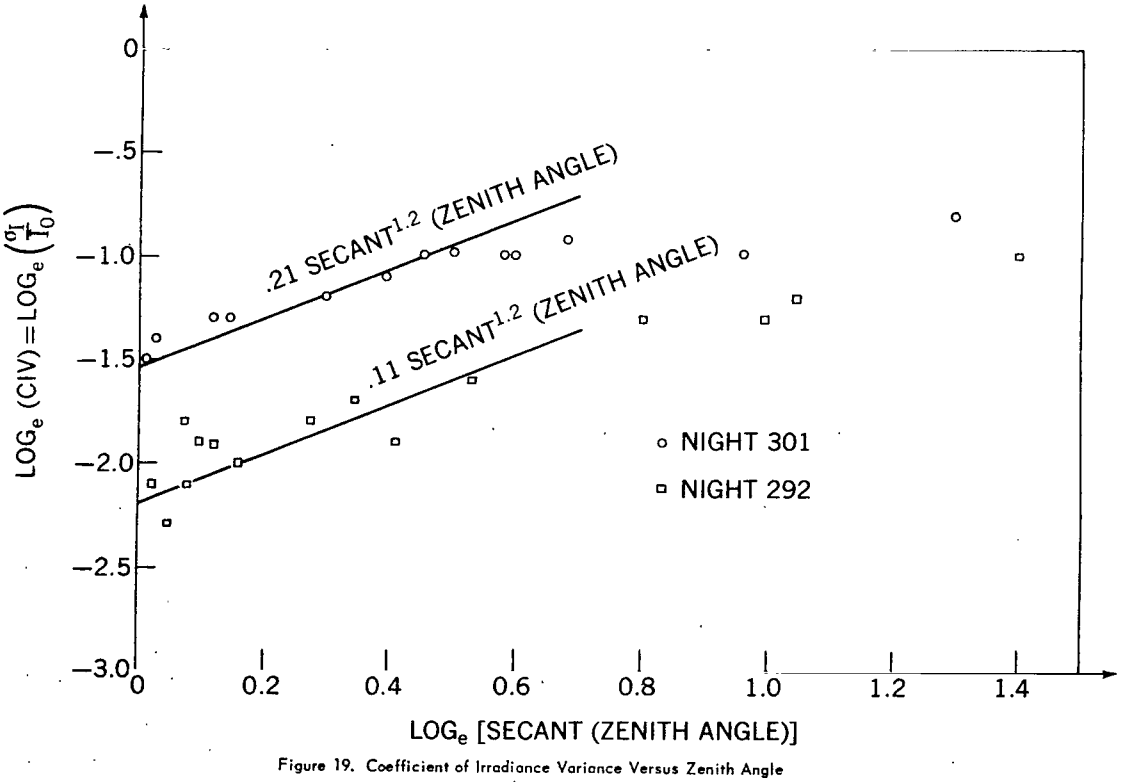

103

Figure 19. Coefficient of Irradiance Variance Versus Zenith Angle

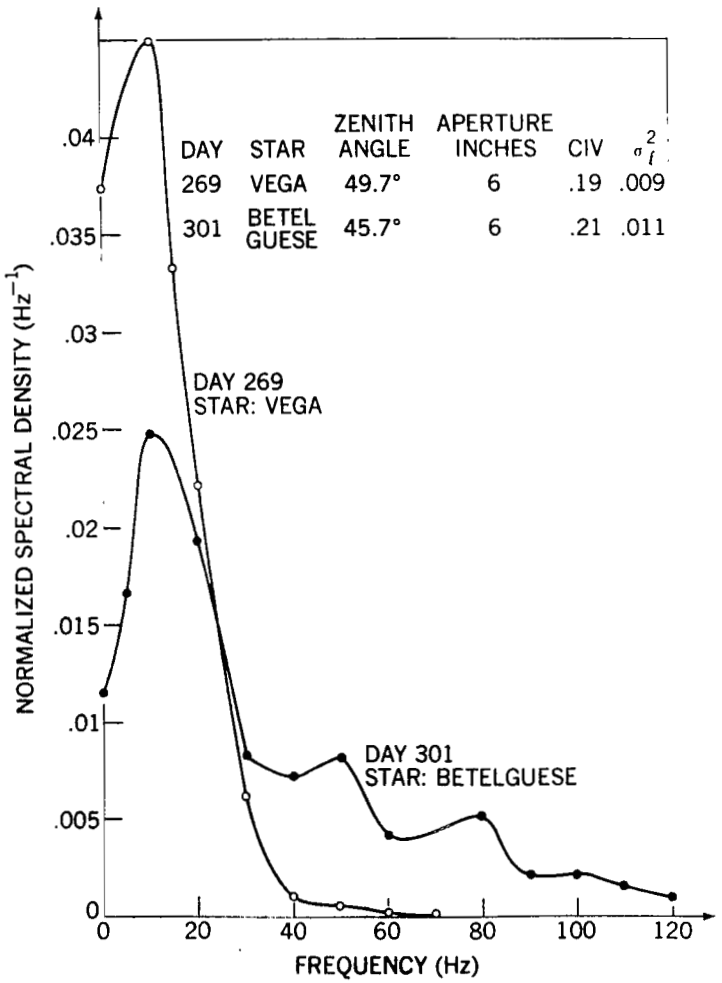

Figure 20. Example of Irradiance Spectral Density Wind Velocity Dependence

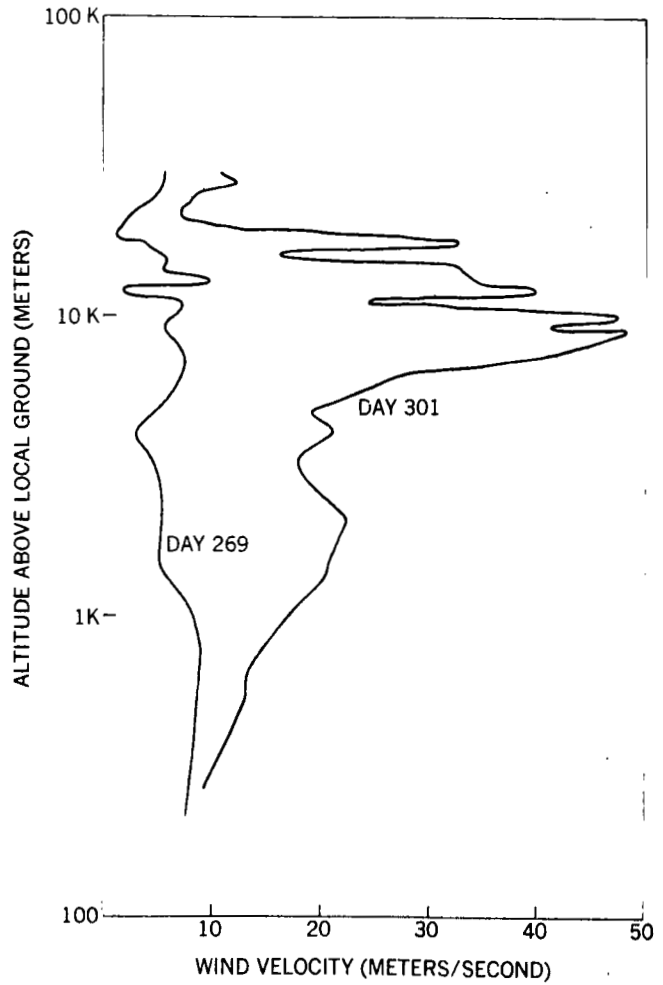

Figure 21. Vertical Wind Speed Profile

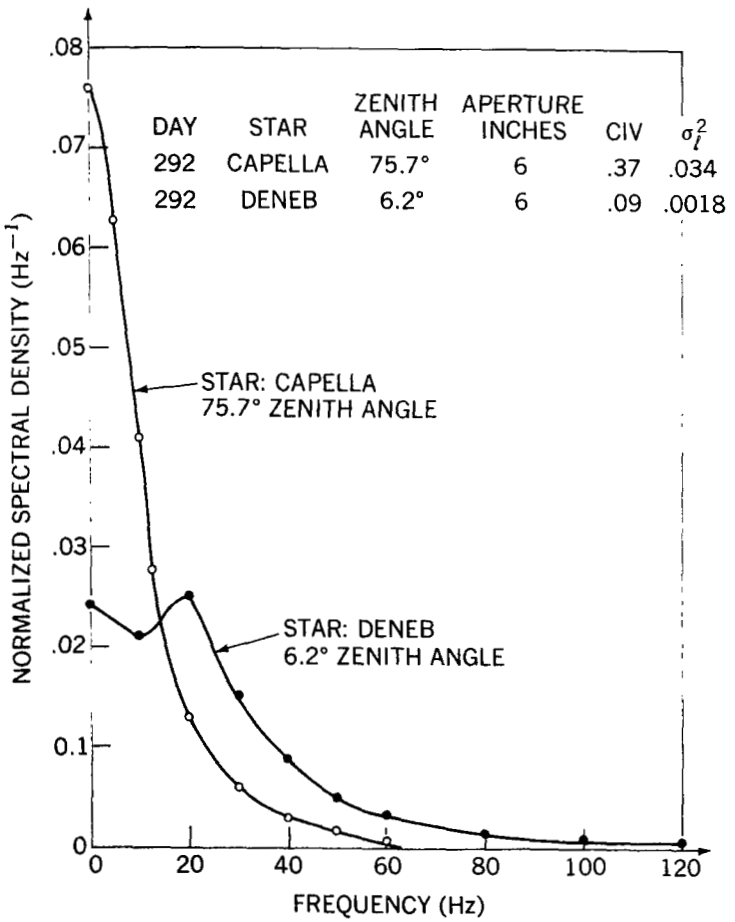

Figure 22. Example of Irradiance Spectral Density Zenith Angle Dependence

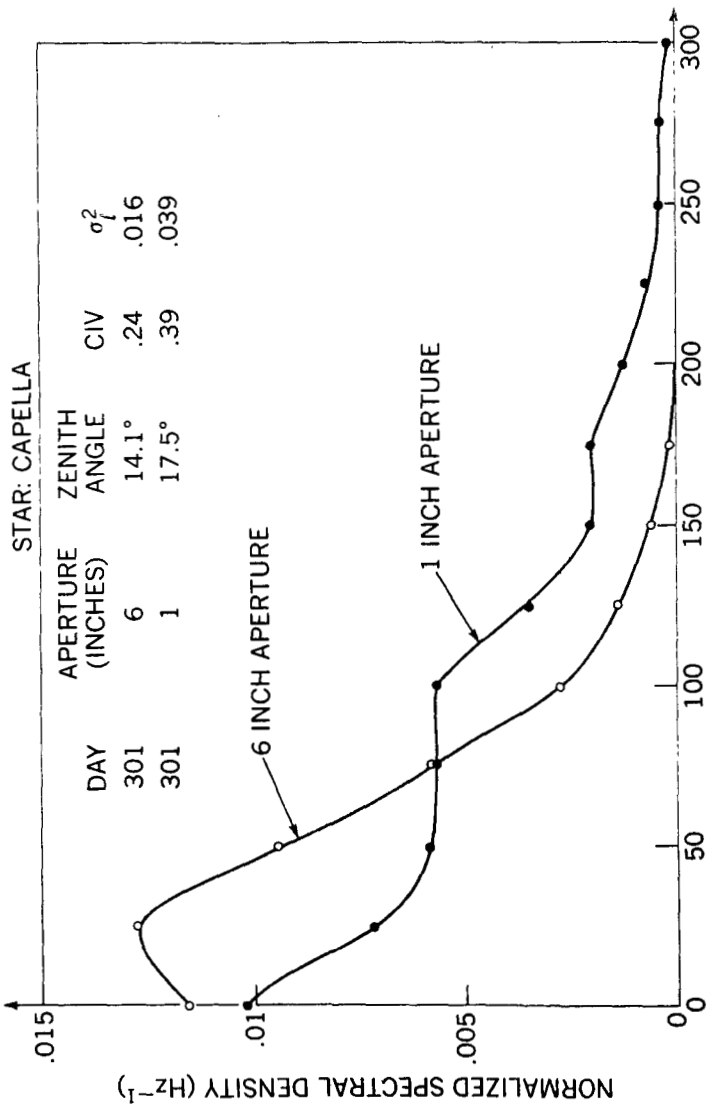

Figure 23. Example of Irradiance Spectral Density Aperture Dependence

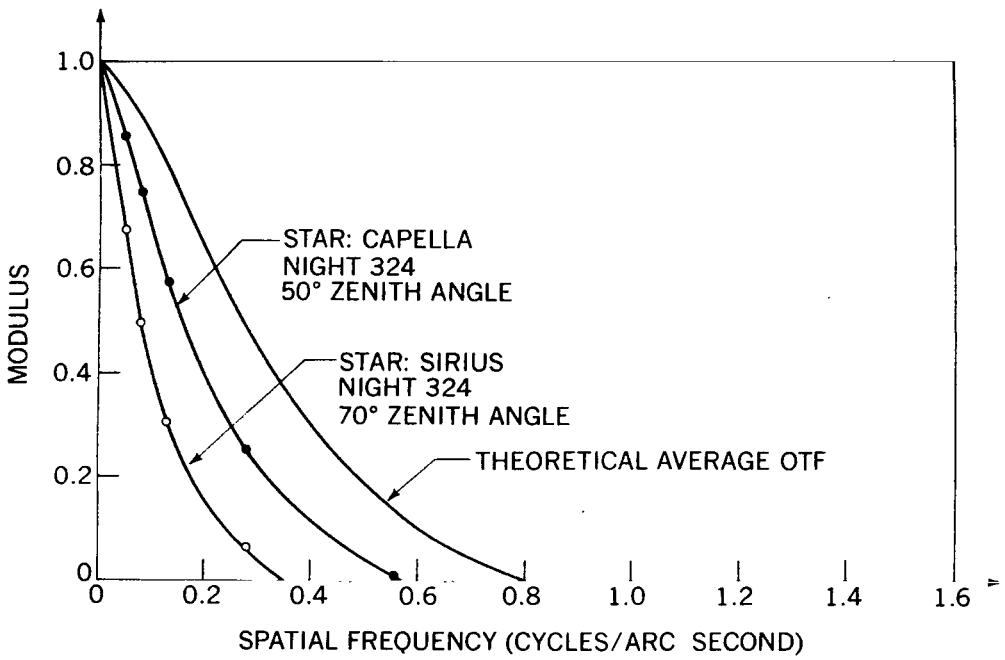

Figure 24. Stellar Optical Transfer Functions

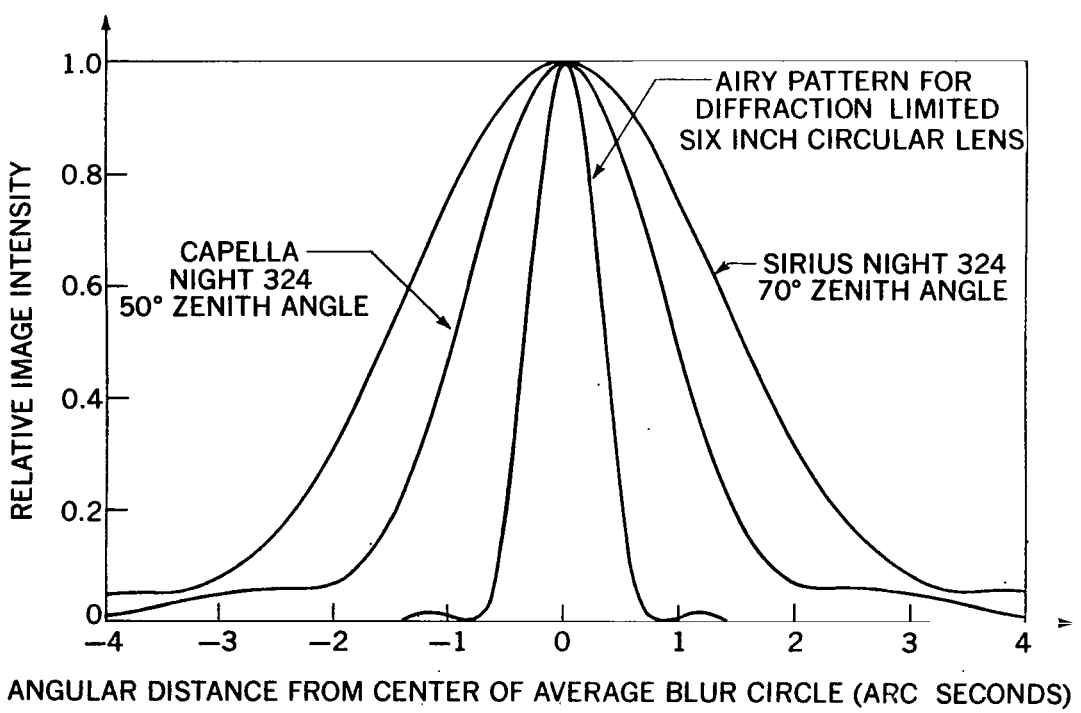

Figure 25. Image Intensity Profiles

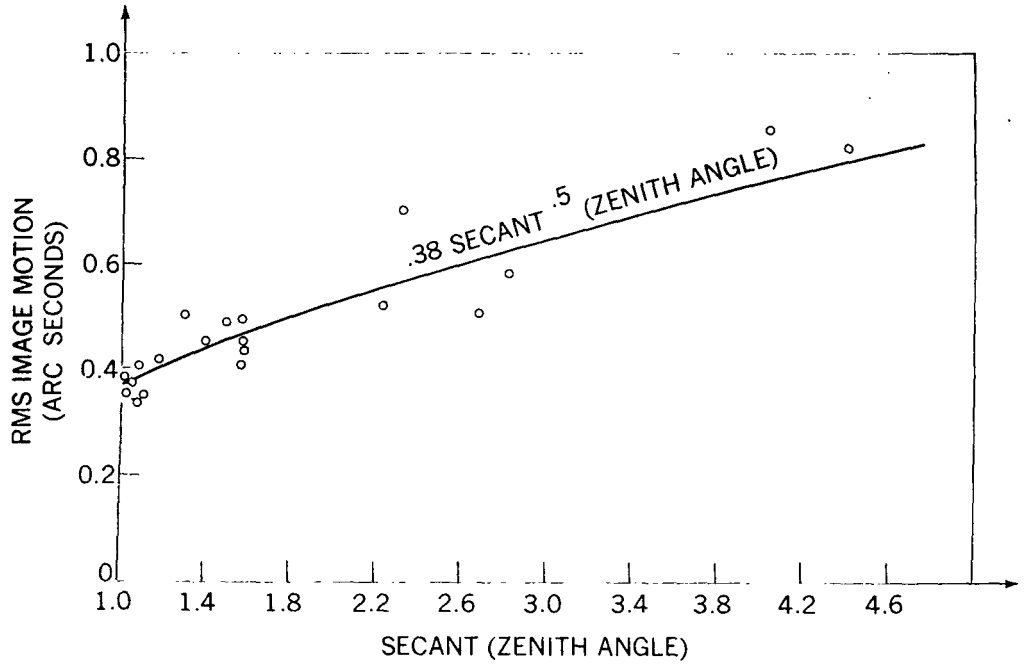

Figure 26. Image Motion Versus Zenith Angle

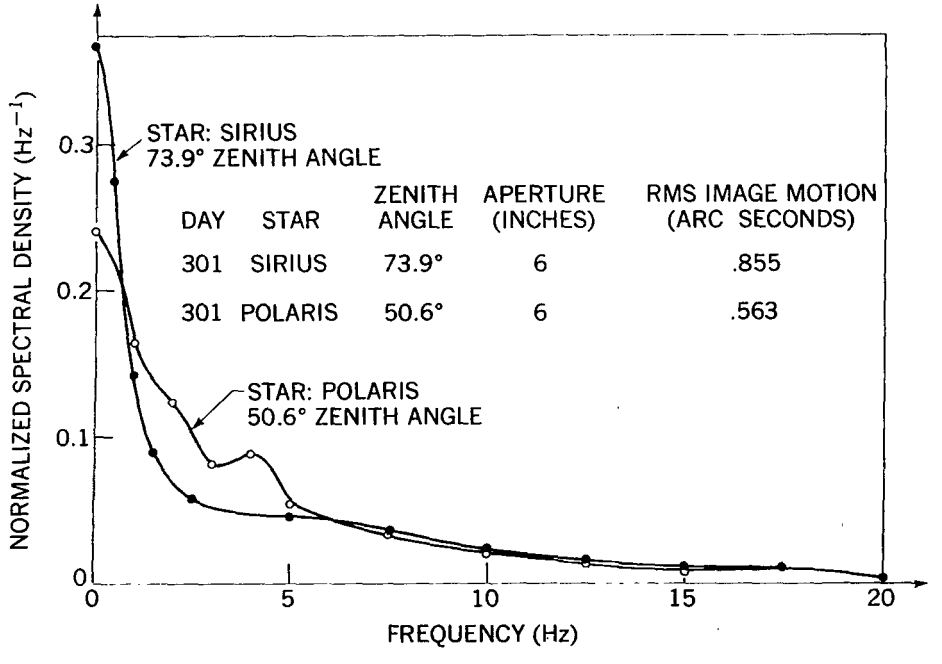

Figure 27. Example of Image Motion Spectral Density